

# Vortex Driven Flame Dynamics and Combustion Instability

by

Hurrem Murat Altay

B.S., Mechanical Engineering  
Middle East Technical University (2003)

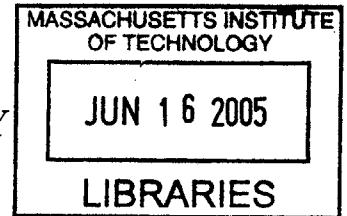
Submitted to the Department of Mechanical Engineering  
in partial fulfillment of the requirements for the degree of

Master of Science in Mechanical Engineering

at the

MASSACHUSETTS INSTITUTE OF TECHNOLOGY

June 2005



© Massachusetts Institute of Technology 2005. All rights reserved.

Author.....  
Department of Mechanical Engineering  
May 6, 2005

Certified by.....  
Ahmed F. Ghoniem  
Professor  
Thesis Supervisor

Accepted by.....  
Lallit Anand  
Chairman, Department Committee on Graduate Students

**BARKER**

# Vortex Driven Flame Dynamics and Combustion Instability

by

Hurrem Murat Altay

Submitted to the Department of Mechanical Engineering  
on May 6, 2005, in partial fulfillment of the  
requirements for the degree of  
Master of Science in Mechanical Engineering

## Abstract

Combustion instability in premixed combustors mostly arises due to the coupling between heat release rate dynamics and system acoustics. It is crucial to understand the instability mechanisms to design reliable, high efficiency, low emission gas turbine combustors. In this thesis, elementary processes acting as a source of unsteady heat release rate are described. These elementary processes are acoustic wave-flame interactions, flame-vortex interactions, equivalence ratio fluctuations, flame-wall interactions and the unsteady stretch rate. To investigate the flame-vortex interaction mechanism, a parametric study is performed in single and double expansion dump combustors. 2-D simulations are performed using the random vortex method combined with thin flame model of premixed combustion. The inlet velocity of the combustor is forced sinusoidally at various amplitudes and frequencies, and the heat release rate response is evaluated. It is shown that the heat release rate dynamics are governed by the cyclical formation of a large wake vortex and its interaction with the flame. Maximum heat release rate in a cycle is reached a short time after the breakup of the vortex, which causes rapid burning of the reactants trapped within the structure. The geometry and operating conditions of the combustor control the mechanism by which the vortex breakup is initiated. For short cavities, the impingement of the large wake vortex onto the forward facing step is responsible for the vortex breakup. On the other hand, in long cavities, the vortex breakup is initiated as the wake vortex impinges on the upper cavity wall in single expansion dump combustor, or the vortex forming in the other half of the combustor in double expansion dump combustor.

Furthermore, the effect of the air injection in the cross stream direction close to the dump plane on equivalence ratio is investigated. It is shown experimentally that high amplitude pressure oscillation in the combustor during unstable operation causes fluctuation in the injected jet velocity. The oscillatory jet velocity affects the incoming equivalence ratio depending on the momentum ratio of the jet to the primary stream. A critical momentum ratio is defined at which the amplitude of the equivalence ratio oscillations reaches a maximum.

Thesis Supervisor: Ahmed F. Ghoniem  
Title: Professor

# Acknowledgments

First, I would like to thank Professor Ghoniem for his guidance and support through the past two years.

I owe a great deal to my colleagues, Daehyun Wee, Sungbae Park, Raymond Speth and Zia Sobhani. Daehyun and Sungbae shared their valuable time for the discussion on the topics in this thesis. Our small discussions with Ray and Zia about research and other general issues gave me new ideas and widened my way of looking at the things.

I am very grateful to my parents, Ismail and Sule Altay for raising me with unconditional love, to my sister Arzu for her help and advices and to Sukran Abla for her incredible understanding and emotional support. I also want to thank to my grandparents, my uncles Osman and Huseyin and their families.

Finally, special thanks to my fiancee Lutfiye for her patience and endless love. Without her it was impossible to withstand everything that I have been through during the past two years.

This work has been sponsored by the Office of Naval Research Advanced Propulsion Program, contract no N00014-99-1-0448 and the Department of Energy Office of Science, contract no DE-FG02-98ER25355.

# Contents

<b>1</b>	<b>Review of Combustion Instability</b>	<b>11</b>
1.1	Reacting Flow Acoustics . . . . .	13
1.2	Elementary Processes As A Source of Unsteady Heat Release Rate . . . . .	15
1.2.1	Acoustic Wave-Flame Interactions . . . . .	15
1.2.2	Flame-Vortex Interactions . . . . .	26
1.2.3	Equivalence Ratio Fluctuations (Mixture Inhomogeneities) . . . . .	34
1.2.4	Flame-Wall Interactions . . . . .	40
1.2.5	Unsteady Stretch Rate . . . . .	43
1.3	Summary . . . . .	46
<b>2</b>	<b>Numerical Investigation of Flame-Vortex Interactions</b>	<b>47</b>
2.1	Numerical Method . . . . .	48
2.2	Results and Discussions . . . . .	50
2.2.1	Double expansion dump combustor . . . . .	51
2.2.2	Short Cavity . . . . .	51
2.2.3	Long Cavity . . . . .	57
2.2.4	Single expansion dump combustor . . . . .	61

2.3	Summary . . . . .	65
<b>3</b>	<b>Effect of the Air Injection in Cross Stream Direction on Equivalence Ratio</b>	
	<b>Oscillations</b>	<b>67</b>
3.1	Experimental Setup . . . . .	68
3.2	Experimental Results . . . . .	69
3.3	Modeling of Combustor Acoustics . . . . .	74
	3.3.1 Modeling of the Combustor Channel . . . . .	74
	3.3.2 Modeling of the Secondary Air Line . . . . .	77
	3.3.3 Equivalence Ratio . . . . .	78
3.4	Modeling Results . . . . .	78
3.5	Summary . . . . .	83
<b>4</b>	<b>Conclusions</b>	<b>84</b>

# List of Figures

1-1	Schematic diagram of combustion instability coupled by acoustic feedback. From Ref. [1] . . . . .	12
1-2	Amplitude and phase dependence of normalized mass burning rate response to acoustic pressure perturbations. From Ref. [13] . . . . .	18
1-3	Schlieren images. Steady conical flame(top), modulation frequency: 75 Hz (bottom). From Ref. [27] . . . . .	20
1-4	Comparisons between analytical predictions and experimental results for the flame transfer function. $(F, \phi)$ is the exact model, and $(H, \phi)$ is the first-order approximation. From Ref. [27] . . . . .	21
1-5	Schematic of the configuration used by Lee et al. From Ref. [29] . . . . .	22
1-6	Transfer functions of conical flame, model A with axial uniform velocity perturbation, model B with perturbation velocity convected in axial direction and symbols are experimental measurements. From Ref. [31] . . . . .	23
1-7	Dependence of the normalized fluctuating $CH^*$ level (denoted by E) upon the normalized fluctuating pressure amplitude (235 Hz driving). From Ref. [36] . . . .	25

1-8	Observations of vortex structures in unstable combustors. (a) High frequency "screech frequency" instability.(b) Low frequency instabilities in a backward facing step geometry. (c) Low frequency instability in a dump combustor. (d) Large scale vortices in a premixed shear layer. (e) Vortex driven instability in a multiple jet dump combustor. (f) Vortex driven oscillations in a single jet dump combustor. (g)Organized vortex motion in a premixed ducted flame modulated by plane acoustic wave. (h)Control of a dump combustor using organized vortices. (i) Vortex motion during the injection phase of a pulse combustor. From Ref. [38]	26
1-9	Schematic of ramjet combustor model used in Ref. [44]	28
1-10	High Speed CCD Images and Linear Photodiode Images captured at 500 Hz, and represent one pressure cycle. From Ref. [46]	30
1-11	Schematic of a swirl stabilized combustor. From Ref. [49]	31
1-12	Flame and Vortex Interaction over one cycle of 1T mode of oscillation. From Ref. [49]	32
1-13	Schematic showing the time evolution of disturbances responsible for a combustion instability. From Ref. [56]	35
1-14	Dependance of instability regions (hatched regions) upon $\tau_{conv,eff}/T$ for several different combustor configurations. From Ref. [56]	36
1-15	Transfer function magnitude and phase upon Strouhal number From Ref. [13]	38
1-16	Pressure and equivalence ratio frequency spectra at Re=5300 and $\phi=0.85$ and in cases I and II. From Ref. [58]	39
1-17	Pressure and equivalence ratio frequency spectra at Re=8500 and $\phi=0.65$ and in cases I and II. From Ref. [58]	39
1-18	Experimental setup. A premixed flame interacts with a plate. From Ref. [59]	41

1-19	Noise measured as a function of driving frequency. $\bar{u} = 1.44m/s$ , $\phi = 0.95$ , burner – platedistance = 7.6mm. WP: with plate, NP: without plate, WC: with combustion, NC: no combustion and LAB: mean background noise in the laboratory. From Ref. [59] . . . . .	41
1-20	Different views of the flame: a)Steady-state, and b-e)instantaneous images of the flame during an instability cycle. From Ref. [60] . . . . .	42
1-21	Location of an oscillated methane/air flame, showing the reduced response with increasing frequency. From Ref. [62] . . . . .	45
2-1	Flame images in a typical cycle . . . . .	52
2-2	Velocity and heat release rate oscillations. $q_m$ is the average heat release rate. Points correspond to the images in Fig. (2-1) . . . . .	52
2-3	Flame images in an unstable cycle from Ref. [44] . . . . .	54
2-4	Flame images at the instance when $\frac{\tau_{conv}U}{D} = 4$ for various $St$ and $S_u$ values. First column (A) and second column (B) correspond to $S_u=0.0125$ and $S_u=0.015$ , respectively. From top row(1) to bottom row(5) the figures correspond to $St$ values, 0.08, 0.095, 0.113, 0.13 and 0.15, respectively . . . . .	55
2-5	$\phi_{q'-u'}$ (in degrees) vs $St$ for different $S_u$ values. Curves are the predictions of the model in eqn. (2.10) . . . . .	56
2-6	Flame images in a typical cycle . . . . .	57
2-7	Velocity and heat release rate oscillations. Points correspond to the images in Fig. (2-6) . . . . .	58
2-8	$\phi_{q'-u'}$ (in degrees) vs $St$ for different $S_u$ values. Curves are the predictions of the model in eqn. (2.11) . . . . .	60
2-9	$r$ vs $St$ for for various cavity geometries . . . . .	61
2-10	$\phi_{q'-u'}$ (in degrees) vs $St$ for Re=2300 and 8400 at constant $S_u$ and density ratio . . . . .	62



2-11	$\phi_{q'-u'}$ (in degrees) vs $St$ for various $S_u$ and density ratios. Amplitude of oscillations is 1.3. Straight lines are linear fits . . . . .	63
2-12	$\phi_{q'-u'}$ (in degrees) vs $St$ for various $S_u$ and density ratios. Amplitude of oscillations is 1.1. Straight lines are the linear fits . . . . .	63
2-13	$\phi_{q'-p'}$ (in degrees) vs $St$ for various $S_u$ and density ratios. $\alpha^*=1.3$ . Data points are numerical results. Straight lines are linear fits. . . . .	64
3-1	Schematic of experimental setup . . . . .	68
3-2	Frequency spectra of jet velocity under different forcing amplitudes . . . . .	70
3-3	Effect of air injection on equivalence ratio oscillations, $\alpha=0.5$ . . . . .	73
3-4	Percent reduction in normalized equivalence ratio oscillation amplitude, $\nu$ , as a function of momentum ratio, $\beta$ . . . . .	74
3-5	Normalized equivalence ratio oscillation amplitude, $\nu$ , as a function of momentum ratio, $\beta$ , for various $\alpha$ values. . . . .	79
3-6	Dependence of the overall sound pressure level on the momentum ratio of the air injected near the step, for primary air velocity of 4.4 m/s, and fixed fuel flow rate of 0.66g/s. From Ref. [73] . . . . .	80
3-7	Primary and secondary air velocities and equivalence ratio without and with the air injection at the location of the slot as a function of time when $\beta = \beta_{crit}$ and $\alpha = 0.5$ . . . . .	81

# List of Tables

2.1	Phase between the initiation of vortex breakup and maximum heat release rate ( $\phi_{bur}$ ) for various normalized flame velocity ( $S_u$ ) and Strouhal numbers ( $St$ ) calculated from the simulation results . . . . .	56
2.2	Phase between the initiation of vortex breakup and maximum heat release rate ( $\phi_{bur}$ ) for various normalized flame velocity ( $S_u$ ) and Strouhal numbers ( $St$ ) calculated from the simulation results. $H^*=1.6$ . . . . .	59

# Chapter 1

## Review of Combustion Instability

Combustion instabilities resulting from the resonant interactions between driving heat release mechanisms and feedback acoustic modes constitute a significant problem in the design of continuous combustion processes. The drive towards lean premixed combustion systems, motivated by stricter emissions regulations, increased the incidence of these instabilities, which occurs in a form of self-sustained oscillations within the combustion chamber. These oscillations may cause flame extinction, structural vibration, flame flashback and structural damage. Large number of research studies have been performed to understand the underlying mechanisms of these instabilities, forming a vast literature on this phenomenon. The objective of this chapter is to review combustion dynamics, in terms of the elementary processes of interaction causing combustion instabilities under certain operating conditions.

There are several ways to explain why combustion process in general is susceptible to instabilities [1]. First, the energy density associated with the combustion is quite large; therefore, a small fraction of this energy is sufficient to drive the oscillation. Second, combustion process involves time lags. That is, reactants entering the chamber are converted into the products in a finite time. Systems with delays are more readily unstable. Third, in most practical combustors, which have confined and weakly damped geometries, resonant interactions can readily occur. These factors all favor the establishment of unstable oscillations.

Rayleigh [2] formulated his well known criterion, stating that the oscillations in a combustor

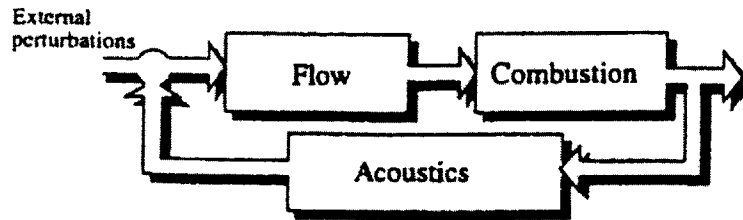


**Figure 1-1: Schematic diagram of combustion instability coupled by acoustic feedback. From Ref. [1]**

are self-sustained if the heat release rate and pressure fluctuations in the combustor are in phase. Therefore, it is important to understand the sources of the unsteady heat release, in order to develop modeling and control strategies. In this chapter, basic elementary processes acting as source of unsteady heat release rate are reviewed. These elementary processes are: flame-acoustic wave interactions, flame-vortex interactions, equivalence ratio fluctuations, flame-wall interactions, and the effects of unsteady stretch rate. In general, heat release fluctuations arise due to the modification of the burning rate at the flame or the modification of the flame's surface area as a result of above processes. There are many other processes which also deserve attention but will not be considered here. For example, in liquid propellant rocket engines, interaction between acoustic waves and droplets or sprays has profound effects, e.g., by inducing tuned breakup of the liquid phase, thus augmenting the rate of vaporization.

Apart from the elementary processes mentioned above, chemical processes are also important in controlling the heat release rate in certain situations. Well Stirred Reactor (WSR) models have been used by several researchers [3, 4, 5, 6] to show the impact of chemical kinetics on heat release rate dynamics. In these models, mixing occurs much more rapidly than chemical kinetics and the reaction occurs homogeneously over the reactor volume.

Reacting flow acoustics will be mentioned briefly, which treats unsteady heat release rate to be the source of the oscillations. The fundamental mechanism for this source is the unsteady gas expansion as the mixture reacts. In general, mutual interaction between the unsteady heat release rate as a source of acoustic perturbations and the perturbations as a source of the unsteady heat

release rate causes combustion instabilities when the heat release rate and pressure oscillations are in phase. Figure (1-1) is a schematic diagram of combustion instability with acoustic feedback. These kind of instabilities require continuous forcing and feedback. However, even in the absence of an acoustic feedback mechanism, self-sustained oscillations at a frequency which may be different than the acoustic frequency can be generated. These kind of instabilities are usually driven by fluid dynamics in the unsteady shear layer [7, 8, 9].

This chapter is organized as follows. Section 1.1 briefly reviews reacting flow acoustics. In section 1.2, elementary processes acting as a source of unsteady heat release are reviewed in detail. In section 1.3, the chapter is ended with a brief summary.

## 1.1 Reacting Flow Acoustics

This section is a brief summary of reacting flow acoustics. Simply, a wave equation relating the unsteady combustion to the acoustic variables is derived and the general form of the solution to this equation is discussed. The intent here is not to provide a full review and description of this complex phenomenon, rather to provide some background material on combustion acoustics. Detailed review of combustion acoustics can be found in Ref. [10].

I start the derivation of the inhomogeneous wave equation from conservation of mass, momentum and energy equations in the absence of external forces [10]:

$$\frac{D\rho}{Dt} + \rho \nabla \cdot \mathbf{u} = 0 \quad (1.1)$$

$$\rho \frac{D\mathbf{u}}{Dt} = -\nabla p + \frac{\partial \sigma_{i,j}}{\partial x_j} \mathbf{e}_i \quad (1.2)$$

$$\rho \frac{D}{Dt} \left( e + \frac{1}{2} \mathbf{u}^2 \right) = -\nabla \cdot (p\mathbf{u}) + q + \nabla \cdot (k\nabla T) + \frac{\partial}{\partial x_j} (\sigma_{i,j} u_i) \quad (1.3)$$

where  $p$  is the pressure,  $\rho$  is the density,  $\mathbf{u}$  is the velocity,  $\sigma_{i,j}$  is the viscous stress tensor,  $D/Dt$  is the material derivative,  $\mathbf{e}_i$  represents the unit vector in the direction of coordinate  $i$ ,  $e$  is the internal energy per unit mass which is  $\int c_v dT$ ,  $k$  is the thermal conductivity and  $q$  is the rate

of heat added to the fluid per unit volume.

Combining eqns. (1.2) and (1.3) and using  $h = \int c_p dT = e + p/\rho$  gives

$$\rho \frac{Dh}{Dt} = \frac{Dp}{Dt} + q + \nabla \cdot (k\nabla T) + \sigma_{i,j} \frac{\partial u_i}{\partial x_j} \quad (1.4)$$

Using the thermodynamic relation  $dh = Tds + dp/\rho$ , eqn. (1.4) becomes

$$\rho T \frac{Ds}{Dt} = q + \nabla \cdot (k\nabla T) + \sigma_{i,j} \frac{\partial u_i}{\partial x_j} \quad (1.5)$$

Assuming that the flow is inviscid; the fluid behaves as an ideal gas; constant specific heats and neglecting heat conduction, the flow variables are linearized by seperating them into steady uniform mean flow (denoted by overbars) and small perturbation (denoted by primes) terms. Using these simplifications, eqns. (1.1), (1.4) and (1.5) become:

$$\frac{\bar{D}\rho}{Dt} + \bar{\rho} \nabla \cdot \mathbf{u}' = 0 \quad (1.6)$$

$$\frac{\bar{D}\mathbf{u}'}{Dt} + \frac{1}{\bar{\rho}} \nabla p' = \mathbf{0} \quad (1.7)$$

$$\bar{\rho} \bar{T} \frac{\bar{D}s'}{Dt} = q' \quad (1.8)$$

where  $\bar{D}/Dt = \frac{\partial}{\partial t} + \bar{u} \cdot \nabla$ . Combining eqns. (1.6)-(1.8) and using  $s' = c_v p'/\bar{p} - c_p \rho'/\bar{\rho}$  the inhomogeneous wave equation is obtained as:

$$\frac{1}{\bar{c}^2} \frac{\bar{D}^2 p'}{Dt^2} - \nabla^2 p' = \frac{\gamma - 1}{\bar{c}^2} \frac{\bar{D} q'}{Dt} \quad (1.9)$$

where  $c$  is the speed of sound and  $\gamma$  is the specific heat ratio. In eqn. (1.9), the heat release rate fluctuations acts as a source driving the acoustic perturbations in the system. Therefore, the reacting flow acoustics, relating heat release rate fluctuations to acoustic perturbations, is generally responsible for the feedback loop leading to combustion instabilities.

In order to solve the acoustic field in a combustor and the growth rate of the oscillations from eqn. (1.9), models to represent heat release rate dynamics should be developed. This

requires understanding the elementary mechanisms leading to heat release rate perturbations and the relative impact of each mechanism on the heat release rate dynamics under different configurations. Several models can be found in Refs. [10, 11, 12].

Other than acoustic perturbations, heat release rate oscillations also generate entropy waves or local hot spots. If the combustor geometry has downstream contraction, and if the frequency of these entropy waves are low enough for the waves to reach the downstream contraction, the entropy disturbance generates sound. If the flow passes the system unrestricted, i.e. no contraction, the entropy waves simply convect out of the system. Even in the absence of unsteady heat release rate, an acoustic oscillation incident on a flame produces entropy and vorticity disturbances [13]. The basic mechanism for the generation of the vorticity disturbance is the baroclinic mechanism due to the misalignment of the mean density gradient and the fluctuating pressure gradient.

## 1.2 Elementary Processes As A Source of Unsteady Heat Release Rate

Perturbations formed within the combustor cause heat release rate fluctuations. The basic impact of these perturbations is causing unsteady changes in the flame surface area and the rate of burning across local flame elements. This section reviews the most significant elementary processes that act as source of unsteady heat release rate. These elementary processes are: acoustic wave-flame interactions, flame-vortex interactions, equivalence ratio fluctuations, flame-wall interactions and unsteady stretch rate.

### 1.2.1 Acoustic Wave-Flame Interactions

Acoustic disturbances influence the flame in variety of ways. They can be classified into different categories depending on whether they effect the internal structure, such as the local burning rate, or the external structure, such as the surface area, of the flame. The former and latter

categories are usually attributed to pressure, i.e.  $O(p'/\bar{p})$ , and velocity, i.e.  $O(u'/\bar{u})$ , coupled mechanisms, respectively. A simple order of magnitude analysis, assuming acoustic scaling, i.e.  $p' \sim \bar{\rho}\bar{c}u' \sim \bar{c}^2\rho'$ , gives that:

$$O\left(\frac{u'}{\bar{u}}\right) = \frac{1}{M}O\left(\frac{u'}{\bar{c}}\right) \sim \frac{1}{M}O\left(\frac{p'}{\bar{p}}\right) \quad (1.10)$$

Therefore, the impact of velocity-coupled mechanisms are larger than pressure coupled mechanisms, in the order of the inverse of the mean flow Mach number. It is important to note that it may not be sufficient to decide the relative effect of various processes on combustion instability by a simple analysis as the one demonstrated above. For example, even if there is a velocity coupled mechanism, Rayleigh's criterion, which is mentioned before, must be satisfied in order to generate significant acoustic energy to form self-sustained pressure oscillations.

A large number of studies have considered various fundamental aspects of the acoustic wave-flame interaction problem. Several studies have been performed to calculate the reflection and transmission coefficients of a planar flame and examined the damping or amplification characteristics of an acoustic wave interacting with a flame, depending on various system conditions. The first study in this area was performed by Chu [14]. He considered the response of an infinitely long flat flame to normally impinging acoustic waves by performing a one-dimensional analysis. Lieuwen [15] generalized Chu's work by investigating the interactions between an obliquely incident acoustic wave on a flame front. His work introduced the additional phenomena of flame wrinkling and vorticity production into Chu's problem.

Furthermore, several studies have been carried out to investigate the interaction of an acoustic wave with wrinkled, turbulent flames [16, 17, 18, 19]. Lieuwen [16] performed a theoretical analysis of acoustic wave scattering by turbulent premixed flames with moving, convoluted fronts that have random characteristics. He assumed that the local flame front curvature was much larger than the acoustic wavelength. Thus, he considered the interactions between flames and high frequency disturbances. He showed that the spectral characteristics of the waves scattered from weakly corrugated flames were the same as those of the incident frequency shifted spectrum of the flame front position. Therefore, scattering measurements can provide information about the spectrum of flame front position for weakly corrugated flames. In a later study [17], he used the same assumptions but accounted for the effects of pressure disturbances upon the



mass burning rate. The solutions were obtained for a coherent scattered field and results from laminar and turbulent flame acoustic wave interactions were compared. He demonstrated that the wrinkled characteristics of turbulent flames served as a source of damping of coherent acoustic energy. A later experimental study by Lieuwen et al. [18] confirmed theoretical predictions that the coherent acoustic wave impinging on a turbulent flame generated narrowband incoherent oscillations about the incident wave frequency. Laverdant et al. [19] numerically studied the interaction of a  $H_2/O_2/N_2$  turbulent premixed flame with a Gaussian acoustic wave. They solved 2-D compressible flow with DNS, taking into account chemical kinetics and transport. Their results showed that for small zones where local Rayleigh's variable was positive, the acoustic wave was amplified. As a whole, the perturbations induced on the heat release rate by the propagation of an acoustic wave thorough a wrinkled turbulent flame appeared to be weak. The flame front was not effected much from the presence of the acoustic wave, however, the wave front itself became wrinkled in a way similar to the flame front during its interaction with the reaction zone, which is in agreement with the conclusion of Lieuwen on wave scattering by turbulent flames [16].

Since the goal of this section is to examine the effects of acoustic perturbations on the unsteady heat release rate, from now on, studies on heat release rate response of flames are examined in detail.

Several studies have analyzed the internal structure of a flat flame which is perturbed by an acoustic wave. These studies have related the flame's burning velocity to the unsteady pressure and temperature variations in the incident wave in the limit of high activation energy. Therefore, these studies in general investigate the pressure coupled mechanism of heat release rate oscillations. McIntosh [20] summarized the results of the previous studies, depending on length and time scales of the acoustic wave and the flame preheat and reaction zones. He defined the following ratios:

$$\tau \equiv \frac{\text{diffusion time}}{\text{acoustic time}} \tag{1.11a}$$

$$N \equiv \frac{\text{acoustic wavelength}}{\text{diffusion length}} \tag{1.11b}$$

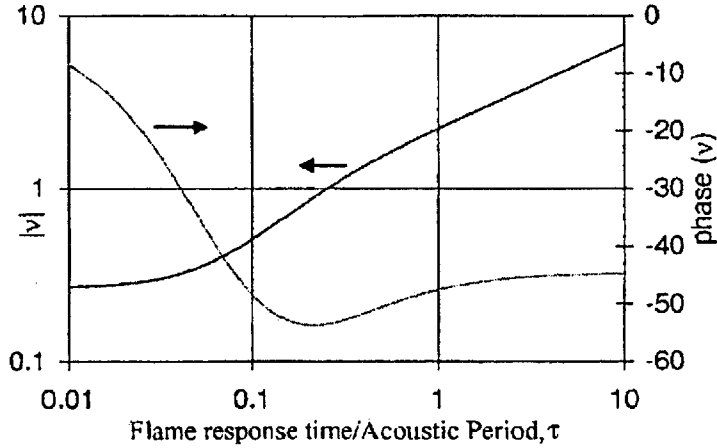


**Figure 1-2: Amplitude and phase dependence of normalized mass burning rate response to acoustic pressure perturbations. From Ref. [13]**

These two quantities are related by the Mach number of flame burning velocity:

$$\tau = \frac{1}{NM_s} \quad (1.12)$$

He then identified four different regimes depending on the relative magnitude of the above defined parameters. Two of these regimes are of most interest to unstable combustors:

1)  $N \gg 1/M_s$ , that is,  $\tau \ll 1$ ; acoustic wavelength is much longer than the flame thickness and the flame responds in a quasi-steady manner to acoustic disturbances.

2)  $N \sim O(1/M_s)$ , that is,  $\tau \sim O(1)$ ; acoustic wavelength is much larger than flame thickness, but the acoustic and flame response times are comparable.

McIntosh [21] expressed the normalized mass burning rate response, i.e.  $\nu \equiv (\frac{m'}{m})/(\frac{p'}{p})$ , for these two regimes as a function of  $\tau$ , dimensionless activation energy ( $\theta$ ), Lewis number ( $Le$ ), specific heat ratio ( $\lambda$ ) and temperature ratio across the flame ( $\Lambda$ ). Figure (1-2) shows the amplitude and phase dependence of the normalized mass burning rate response on  $\tau$  for the parameters defined above. It is observed that the mass burning rate response is substantially larger than its quasi steady value in  $\tau \sim O(1)$  case.

Another mechanism causing unsteady heat release rate by acoustic perturbations is the fluc-

tuation of the flame surface area. As mentioned in the beginning of this section, flame area fluctuation is a velocity coupled mechanism of heat release rate oscillations. This mechanism was investigated in the literature analytically, experimentally and numerically by various authors, by modulating an initially stable flame by acoustic waves in realistic geometries. If the process remains in the linear range, transfer functions can be calculated between the velocity and heat release rate fluctuations. Early studies [22, 23, 24] indicate that the transfer functions act like a low-pass filter. In analytical studies, the flame front is treated as a surface of discontinuity between reactants and products whose instantaneous surface is described by the parametric equation  $G(\mathbf{x}, t) = 0$  [25]. The unit normal to the flame surface is  $\mathbf{n}_f = \nabla G / |\nabla G|$ . Moving along the trajectories of the points defining the flame front,  $G = \text{constant}$ , and thus

$$\frac{dG}{dt} = \frac{\partial G}{\partial t} + \nabla G \cdot \frac{d\mathbf{x}}{dt} = 0 \quad (1.13)$$

where  $\frac{d\mathbf{x}}{dt}$  is the flame velocity. The flame front consumes the reactants located on the  $G < 0$  side by moving in the normal direction at the laminar burning velocity  $S_L$ . It is also convected by the incident flow velocity  $\mathbf{u} = (u, v)$ . Therefore, the flame speed is:

$$\mathbf{V}_f = \frac{d\mathbf{x}}{dt} = \mathbf{u} - S_L \frac{\nabla G}{|\nabla G|} \quad (1.14)$$

Substituting this into eqn. (1.13) gives the following equation governing the evolution of the flame surface:

$$\frac{\partial G}{\partial t} + \mathbf{u} \cdot \nabla G = S_L |\nabla G| \quad (1.15)$$

Further formulation for different geometries can be found in Refs. [26, 27, 28]. Numerical studies divide the flame motion into advection and burning contributions. Advection,  $\partial G / \partial t + \mathbf{u} \cdot \nabla G = 0$ , and burning,  $\partial G / \partial t = S_L |\nabla G|$ , are handled using a level set method for tracking the flame front and a proper numerical scheme to compute the gradients. Experimentally, the flow is modulated using a loudspeaker at the desired amplitude and frequency.

Fleifil et al. [26] developed an analytical model for an axisymmetric flame in a duct, both in uniform and non-uniform imposed velocity conditions. They found that the flame response to applied incidence oscillations was primarily controlled by the forcing frequency ( $\omega$ ). Therefore,

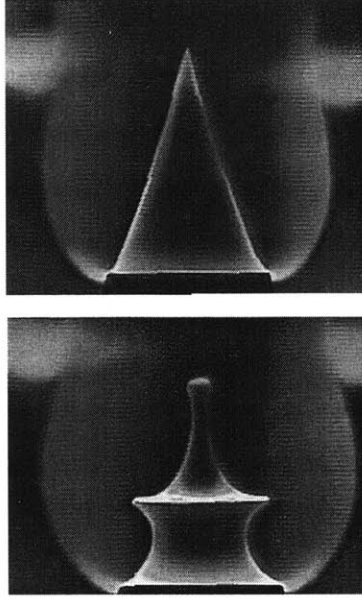


**Figure 1-3: Schlieren images. Steady conical flame(top), modulation frequency: 75 Hz (bottom). From Ref. [27]**

the transfer functions are given in the form:

$$F(\omega) = \frac{(Q'/\bar{Q})}{(u'/\bar{u})} \quad (1.16)$$

Ducruix et al. [27] used the assumptions of Fleifil et al, but extended their study to account for operating conditions leading to conical flames. Figure (1-3) shows the Schlieren images that they obtained from their experiments on stable and modulated conical flames. Their model suggests that the unsteady flame characteristics can be described using a single parameter in a form of reduced frequency,  $\omega^* = \omega R / S_L \cos \alpha_o$ , where  $\omega$  is the forcing frequency,  $R$  is the burner radius,  $S_L$  is the laminar burning speed and  $\alpha_o$  is the half cone angle of the steady flame. Figure (1-4) compares the magnitude and phase of their calculated and measured transfer functions. For  $\omega^* > 6$  the predicted phase of the transfer function does not match with the experiment. The analytical prediction of the magnitude of the transfer function have a good match with the experiments; however, the models do not capture the non-monotonic behavior observed when  $\omega^* > 8$ .

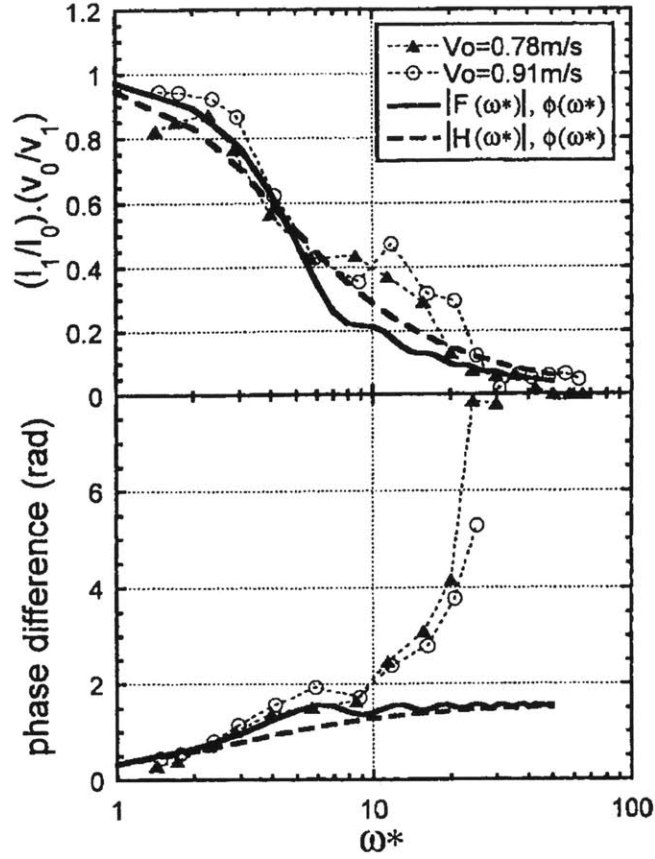


Figure 1-4: Comparisons between analytical predictions and experimental results for the flame transfer function.  $(F, \phi)$  is the exact model, and  $(H, \phi)$  is the first-order approximation. From Ref. [27]

In Ref. [30], Lee et al. showed that multi-dimensional effects of the acoustic field were important near the flame. In a later numerical study [29], they considered two dimensional acoustic field in a near flame zone as shown in Fig. (1-5). They compared their results with the one dimensional analytical model used by other authors. They showed that multi-dimensionality did not exert substantial qualitative differences between one and two dimensional calculations. The little discrepancy between the two results were shown to be the result of gas compressibility in the flame region and spatial nonuniformity of the acoustic velocity along the flame front.

Schuller et al. [28] developed an analytical model based on the linearization of the G-equation for an inclined flame. They also included the convective effects of the flow modulations propagating upstream of the flame. They showed that flame dynamics was controlled by two parameters:

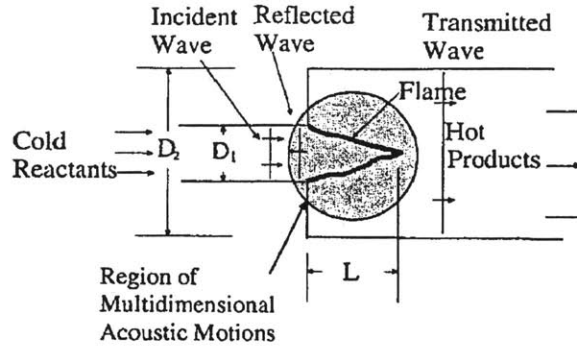


Figure 1-5: Schematic of the configuration used by Lee et al. From Ref. [29]

the forcing frequency ( $\omega$ ) as defined in the earlier studies and the flame angle  $\alpha$  (or  $S_L/\bar{v}$ ) with respect to the flow direction. Previous kinematic models with uniform forcing velocity are limiting (low frequency) case of their model. They compared conical and V-flame dynamics. The conical flame behaved as a low pass filter and was not too sensitive to the amplitude of the incident velocity perturbation. However, the V-flame responded strongly to the amplitude of velocity perturbations and had a preferred range of frequencies where it acted as an amplifier. Therefore, they claimed that the V-flame was more susceptible to combustion instabilities.

In Ref. [31], Schuller et al. carried out combined numerical and experimental analyses for conical flames as a continuation of their previous study. As in the earlier study they used two different models for flow modulation. In the first model, they forced the flow with uniform harmonic velocity, in the second, they included convective effects on flow modulations. The equations for the velocity field  $\mathbf{u}(u, v)$  in fresh mixture for the two models are [31]:

Uniform velocity modulation:

$$v = \bar{v} + \sqrt{2}v_{rms}\sin(\omega t) \quad (1.17a)$$

$$u = 0 \quad (1.17b)$$

where  $\omega$  is the forcing frequency and  $v_{rms}$  is the root mean square velocity modulation measured 1.5 mm above the burner outlet.

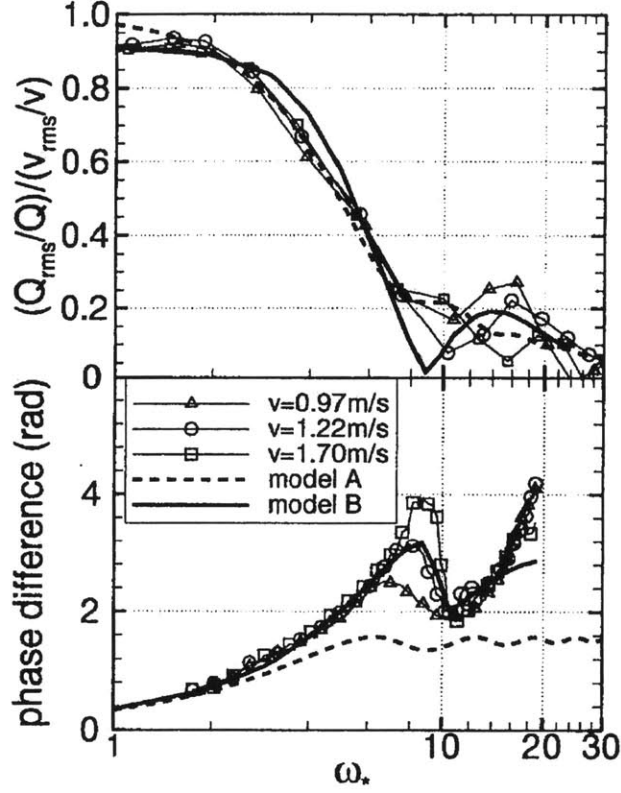


Figure 1-6: Transfer functions of conical flame, model A with axial uniform velocity perturbation, model B with perturbation velocity convected in axial direction and symbols are experimental measurements. From Ref. [31]

Velocity modulation with convective effects:

$$v = \bar{v}\sqrt{2}v_{rms}(y)\sin(\omega t - ky) \quad (1.18a)$$

$$u = \frac{x\sqrt{2}}{2}\left[v_{rms}(y)k\cos(\omega t - ky) - \frac{dv_{rms}}{dy}\sin(\omega t - ky)\right] \quad (1.18b)$$

where  $k$  is the convective wave number ( $\omega/\bar{v}$ ),  $x$  is the radial distance from the burner axis,  $y$  is the axial distance from burner outlet and  $v_{rms}$  is defined before. In Fig. (1-6) they compared their experimental and numerical transfer functions. It is seen that the numerical results with the convective model predicts the flame dynamics much better than the uniform forcing velocity model.

So far the discussion has focused on the linear response of a premixed flame to small-amplitude

perturbations. However, it is critical to understand the nonlinear response of flames to finite amplitude perturbations to predict the limit-cycle amplitudes. Most of the older work considering the nonlinear response [32, 33] focused on the role of nonlinear gas dynamics in combustors. As such, it is likely to be more relevant to instabilities where the fluctuating pressure amplitudes achieve significant percentages of the mean, i.e.  $p'/\bar{p} \sim 0.2-0.5$ , much higher than encountered in lean premixed gas turbine combustors where the reported instabilities are typically in the order of 0.01-0.05 of the mean pressure. Recent studies suggest that the nonlinear gas dynamics processes are not relevant in gas turbine combustors.

Bourehla et al. [34] experimentally studied the response of conical premixed methane/air flame under a wide range of forcing frequency and amplitudes. In particular, they found that the flame did not oscillate at the same frequency as the flow, which responded always to the acoustic frequency. At low frequencies ( $f < 200Hz$ ) and amplitudes ( $u'/u < 0.3$ ), the flame front wrinkled always about the burner axis due to a convected wave traveling from the burner base to the tip. At higher frequencies but same amplitudes, the effect of oscillations were only evident at the flame base and damped at axial locations further downstream. This behavior may be due to the increased importance of the flame's curvature-dependent burning velocity and the very short convective wavelengths of the imposed disturbances at these high forcing frequencies [13]. Finally, at high frequencies and amplitudes the flame collapsed and the tip region became rounded off.

Dowling [35] developed a model for the low-frequency nonlinear response of a ducted V-flame to examine the self-excited oscillations. In order to treat the finite amplitude oscillations, a non-linear boundary condition at the flame anchoring point was utilized. The flame remained attached to the flame holder when the total gas velocity exceeded the flame speed. When the opposite was true, the flame was allowed to move upstream. She observed that weak disturbances grew into limit cycles, which reproduced the experimental observations.

Lieuwen et al. [36] performed an experimental study to characterize the pressure- $CH^*$  relationship as a function of the oscillation amplitude. Their results showed that this relationship was linear for pressure amplitudes below 0.01 of the mean pressure. After this point the heat release rate oscillation amplitude began to saturate. They found that the saturation occurred at



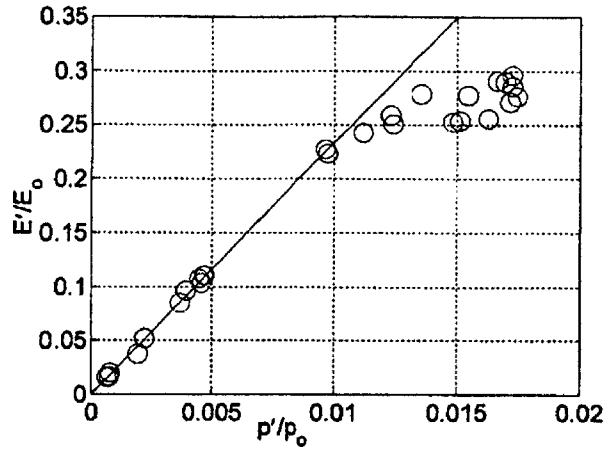


**Figure 1-7: Dependence of the normalized fluctuating  $CH^*$  level (denoted by  $E$ ) upon the normalized fluctuating pressure amplitude (235 Hz driving). From Ref. [36]**

$CH^*/\bar{CH}^*$  values of around 0.25 as shown in Fig. (1-7).

In another study, Bellows et al. [37] obtained simultaneous measurements of  $CH^*$ ,  $OH^*$  chemiluminescence; pressure and velocity over a wide range of forcing amplitudes and frequencies. In some cases they observed saturation of flame chemiluminescence response to imposed pressure/velocity oscillations. Also, the phase between the chemiluminescence and pressure/velocity signal exhibited substantial amplitude dependence. On the other hand, the pressure-velocity relationship remained linear with constant phase over the entire amplitude range. This suggests that the nonlinear relationship between the pressure and heat release oscillations has a more significant role in saturating the amplitude of self-excited oscillations in premixed combustors than the nonlinear gas dynamic processes.

This section is concluded with several remarks. The interactions of an acoustic wave on a planar flame in simple geometries has been extensively studied theoretically and good understanding of the phenomenon is achieved. However, no significant experimental study has been performed to assess the predictions of these studies. This is because of the difficulty of designing an experimental setup that can correctly predict the phenomena occurring in such simple geometries. Large number of analytical, theoretical and numerical studies have been performed to analyze laminar flames and to measure flame transfer functions under acoustic velocity modulation in the linear regime. Simple analytical models accurately predict the experimental results at low

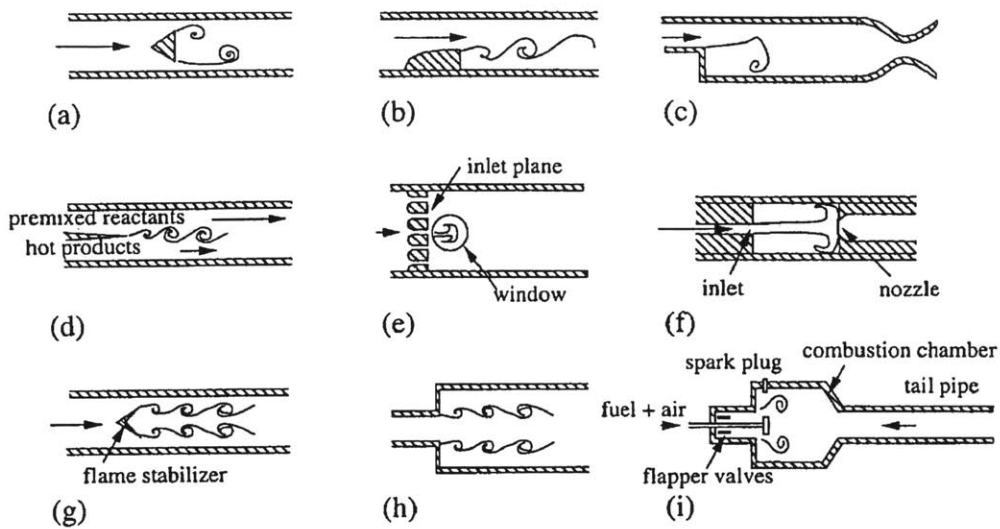


**Figure 1-8: Observations of vortex structures in unstable combustors. (a) High frequency "screech frequency" instability. (b) Low frequency instabilities in a backward facing step geometry. (c) Low frequency instability in a dump combustor. (d) Large scale vortices in a premixed shear layer. (e) Vortex driven instability in a multiple jet dump combustor. (f) Vortex driven oscillations in a single jet dump combustor. (g) Organized vortex motion in a premixed ducted flame modulated by plane acoustic wave. (h) Control of a dump combustor using organized vortices. (i) Vortex motion during the injection phase of a pulse combustor. From Ref. [38]**

forcing frequency cases. For high forcing frequencies more complex numerical tools are required for reliable modeling. The successful studies performed on laminar flames should be extended to turbulent flow conditions with highly perturbed fronts. The effect of increasing turbulence level on the measured transfer functions should be addressed. The investigations of nonlinear combustion dynamics are mostly theoretical. The kinematics of nonlinear flame response is well understood. Attention should also be given to other nonlinear mechanisms such as local flame extinction, global flame extinction, chemical kinetics and equivalence ratio oscillations.

## 1.2.2 Flame-Vortex Interactions

Vortex structures are a major cause of combustion instabilities. Figure (1-8) demonstrates several vortex structures observed in various unstable combustors. The basic mechanism which involves vortices is the rapid change of flame surface area as it interacts with a vortex, thereby causing

heat release rate oscillations. Also, collision of a vortex with a wall or another structure results in the sudden burning of reactants, generating a heat release pulse which feeds energy into the system to support the oscillations.

Several conditions should be satisfied to sustain the instabilities caused by vortical structures. First, according to the Rayleigh's criterion the heat release rate oscillations due to combustion must be in-phase with the pressure oscillations. Also, the unsteady heat release rate should show a peak during a short interval within the instability cycle to feed considerable energy into the acoustic field. The moment of the highest heat release rate has a significant importance in determining the behavior of the system. In most of the combustors operating under lean conditions and involving unsteady vortex shedding, the time of maximum heat release is such that the Rayleigh's criterion is satisfied. The pulsatile nature of combustion oscillations is associated with vortex breakup and intense turbulence-combustion interactions. Furthermore, large acoustic velocity fluctuations must be present at flow separation to have the unsteady vortex formation. Therefore, high acoustic gains are needed and unstable frequencies are mostly determined by the acoustic eigenfrequencies of the combustion system.

Several experimental and numerical studies have been performed to investigate the interaction of vortices with a flame (see Ref. [38] for review). These studies often generate isolated vortex structures and propagate them towards a premixed or strained diffusion flame to investigate the structure of the flame as it is wrapped up around the vortex, the formation of a central core, the secondary vorticity generation, the quenching of reaction zone, the ignition dynamics and combustion enhancement, etc. However, observations of combustion oscillations indicate that both the presence of the flame and the vortex influence each other. That is, the vortex pattern is influenced by the flame presence as it is being generated and also the flame development is influenced by the ignition and delayed combustion of the vortex structures. Therefore, studies of continuous combustion processes in realistic geometries as in Fig. (1-8) have been performed to investigate these complex processes.

Early observations of vortex shedding from flameholders are reported in Refs. [39, 40]. In the last two decades several experimental studies have been performed to examine the self-sustained oscillations controlled by vortices [41, 42, 43, 44, 45, 46, 47]. Poinso et al. [41]

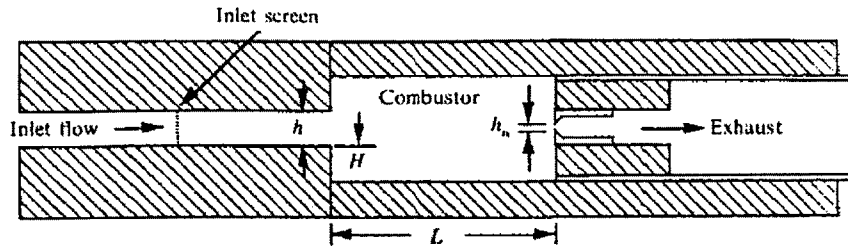


Figure 1-9: Schematic of ramjet combustor model used in Ref. [44]

investigated a multiple inlet dump combustor which was fed with a mixture of air and propane (see Fig. 1-8e). They observed vortex driven, low-frequency instability which was acoustically coupled. As a result of the interaction of adjacent vortices, a combustion pulse was produced creating large amount of small-scale turbulence and flame surface area. The sudden heat release, acting as a source, fed energy into the perturbed acoustic motion. Venkataraman et al. [45] studied the mechanism of unstable combustion in a coaxial bluff-body stabilized dump combustor. Their results also indicated the significant role of flame area fluctuations as a result of flame-vortex interaction in the observed instability for premixed combustion. They also studied the contributions to heat release fluctuations from area, equivalence ratio and pressure oscillations. They found that heat release oscillation was associated with both flame area and equivalence ratio fluctuations, the former having more contribution.

An investigation by Kendrick et al. [48] revealed another mechanism of unsteady heat release rate involving vortices in premixed devices. They observed that collisions of vortices with boundaries induced rapid burning of the fresh reactants entrained by the structure. Also, when vortices consist of only combustion products, the impingement of these structures on a wall induces pressure oscillations into the system. This mechanism is not associated with the unsteady heat release caused by the combustion and usually has a much smaller effect on producing acoustic source compared to the vortex combustion.

Yu et. al. [44] studied combustion instabilities in the model ramjet combustor shown in Fig. (1-9). The facility is composed of a long inlet duct, a dump combustor cavity and an exhaust nozzle. They observed instability over wide range of operating conditions. Schlieren images show that the instability is associated with the large-scale flame front motions which are driven by

periodic vortex shedding at the unstable frequency. Their results indicate that the inlet duct acts as a long-wavelength acoustic resonator. However, the unstable frequency does not lock to any particular value suggesting that the instabilities are not only acoustic in nature. In fact, the instability is due to a mixed acoustic-convective mode. In order to determine how the unstable frequency is selected, they varied the characteristic lifetime of the vortices,  $\tau_v$ , and the acoustic feedback time,  $\tau_f$ , which are related to convective modes and acoustic modes, respectively. In a typical unsteady cycle, the vortices form in the dump plane when the flow acceleration is maximum, grow in size, convect through the combustor cavity and burn as they impinge on the exhaust nozzle. This suggests that the vortex lifetime can be approximated by:

$$\tau_v \sim \frac{L}{U} \quad (1.19)$$

where  $L$  is the combustion cavity length and  $U$  is the mean flow velocity taken to be the vortex convection velocity. On the other hand, the acoustic feedback time characterizes the delayed response of the inlet duct and is the time passing between the maximum heat release rate and the new vortex formation time at the step. Therefore, the instability period is given as:

$$T_i = \frac{\tau_v + \tau_f}{N} \quad (1.20)$$

where  $T_i$  is the instability period and  $N$  is a positive integer representing the mode number. When the acoustic feedback time is significantly large compared to the vortex lifetime, there could be additional vortex shedding before the characteristic response time completely elapses. Then, the instability frequency will be increased from first to higher modes of oscillations.

Combining eqn. (1.20) with Rayleigh's criterion gives the following condition for sustaining an oscillation at mode  $N$ :

$$\frac{1}{4N-1} < \frac{\tau_v}{\tau_f} < \frac{3}{4N-3} \quad (1.21)$$

From eqn. (1.21) it can be seen that mode 1 oscillation requires the ratio between  $\tau_v$  and  $\tau_f$  to be in the range from  $\frac{1}{3}$  to 3 and mode 2 from  $\frac{1}{7}$  to  $\frac{3}{5}$  to establish sustained oscillations. There is a region of overlap between the two modes which may correspond to transition from one mode to the other.

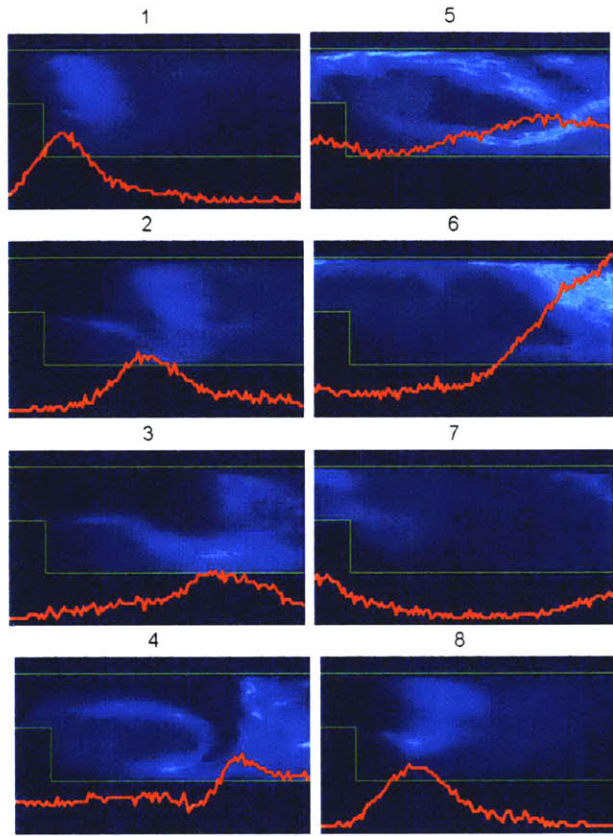


**Figure 1-10: High Speed CCD Images and Linear Photodiode Images captured at 500 Hz, and represent one pressure cycle. From Ref. [46]**

In general, in this study it is shown that both acoustic modes and convective modes can exist together, and together they determine the unstable characteristics of a combustion system. This occurs most often in combustors with closed geometries, such as in the ramjet combustors discussed above. The instability characteristics can be modeled by considering acoustic and convective characteristic time scales, where the former is controlled by the inlet duct geometry and the latter is determined by the vorticity lifetime, in other words, the moment in an unstable cycle where the heat release rate is maximum.

In a recent work, Ghoniem et al. [46] performed an experimental study to examine a premixed flame in a rearward-facing step combustor. The unstable frequency was constant around 40 Hz for different inlet velocities, suggesting the significance of acoustic feedback. Their results showed resonance between the acoustic quarter wave mode of the combustion tunnel and the fluid dynamic mode of the wake. Figure (1-10) is the high speed CCD images they obtained for

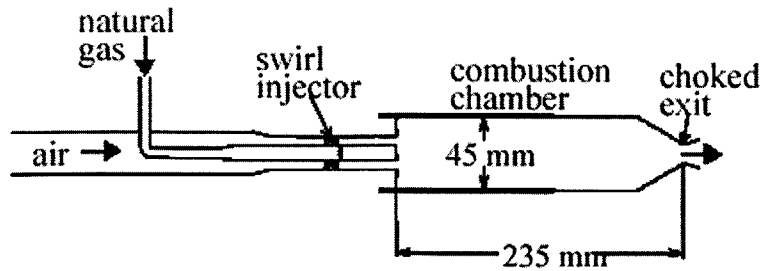


Figure 1-11: Schematic of a swirl stabilized combustor. From Ref. [49]

one cycle. The red lines showing the spatial location of the flame front obtained from a linear photodiode array. The first image in Fig. (1-10) correspond to the maximum upstream velocity, where the flame appears as a vertical front propagating downstream of the step. As the velocity drops, the vortex gets larger and it reaches its maximum size when the velocity is minimum (mostly negative) (4). At that time, the leading edge of the flame folds forming a reactant pocket. Next, while velocity is increasing, heat release increases rapidly as the reactants in the pockets are consumed (5-6), and the vortex collides the upper wall of the combustor generating a sudden increase in the flame area. The cycle ends when the maximum velocity is reached (7-8) and the flame is pushed back towards the step. This cyclical formation of the wake vortex, and its interaction with the flame controls the heat release rate dynamics.

Bernier et al. [47] investigated instability mechanism in a premixed swirl stabilized combustor. They considered two sets of swirling blades that induce flow rotation in the same direction (co-rotative) or in the opposite direction (counter-rotative). The frequencies of combustion instabilities that they observed were mainly defined by the acoustic modes of the system. In the counter rotating geometry, the flow developed large vortical structures that entrained fresh reactants. They ignited at a later time producing a pulse of heat release. This is a typical instability mechanism involving vortices, as mentioned before. In co-rotating configuration no structures were observed. The reaction rate grew as the front propagated downstream. Based on a time-delay analysis they suspected that this instability was due to mixture inhomogeneities (see section 1.2.3).

Numerical studies involving realistic geometries are reported in Refs. [50, 51, 52, 49]. In Ref. [50] Najm and Ghoniem numerically investigated the dynamics of reacting flow in a 2-D cavity-



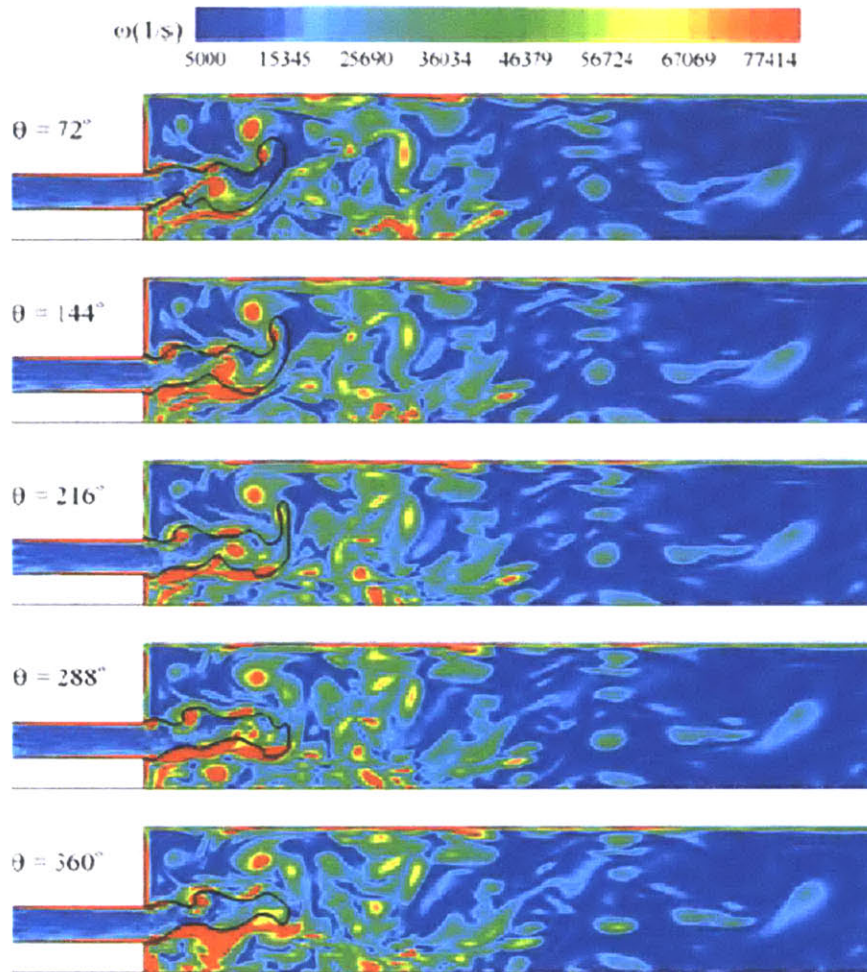


**Figure 1-12: Flame and Vortex Interaction over one cycle of 1T mode of oscillation. From Ref. [49]**

type dump combustor using the random vortex method and flame based combustion model. Their simulations showed that vorticity-flame-acoustic coupling was the driving mechanism of the observed instability. The combustor flow-field was dominated by the organized shedding of large vortical structures from the recirculation zone in the combustor. When they forced the exit pressure of the combustor at low frequency, close to the combustor natural frequency, the recirculation zone instability was amplified. As the rate of heat release was increased, the amplified instability led to flame flashback.

Recent works mostly involve swirl-stabilized combustors, because they are more practical in industrial use. Huang et al. [49] simulated reacting flow in a lean premixed swirl-stabilized



combustor using LES. Figure (1-11) shows the schematic of the combustor geometry. They took into account finite rate chemical reactions and variable thermophysical properties. Premixed flame was simulated using a level-set flamelet library approach. The governing equations in 3-D together with the boundary conditions were solved using a four-step Runge-Kutta scheme. Figure (1-12) shows the flame vortex interaction over one cycle of the first tangential (1T) mode of oscillation in the upper half region. The black line indicates the flame surface. New vortices are produced at the tip of the backward facing-step at  $\theta = 72$  deg, forming a bulge in the flame front. These vortices distort the flame and produce flame pockets when traveling downstream. At the end, these structures move out from the flame region and dissipate into small scale structures. In general, the vortical motions in the flame zone resonate with the acoustic oscillations in the chamber causing large excursions of unsteady motions. The flame is contorted and convoluted by the local flow oscillations, generating unsteady heat release rate in the flame zone driving acoustic waves in the chamber. In terms of the chamber acoustic characteristics and flame shape, good matching with the experiments were obtained.

This section is concluded with some final remarks. Several experimental and numerical studies have been performed to understand the physics of flame-vortex interaction phenomena. Studies involving isolated vortices interacting with a flame have provided details about intrinsic structures of the vortices and the flames as they interact with each other. Studies performed in realistic geometries helped understanding of the combustion instabilities especially involving unsteady vortex shedding mechanism. In general, the unsteady heat release rate is driven by the flame area fluctuations caused by the periodic shedding of the vortical structures in the combustor. The frequency of this unsteady vortex shedding mechanism is mostly determined by the acoustic modes of the system. However, for some cases, especially involving combustors with closed geometries, both acoustic and fluid dynamic modes are significant [44]. Also, there are some studies reporting that the fluid dynamic instabilities of the reacting shear layer define the unstable mode frequency, perturb the heat release and feed energy into the acoustic field, which under the circumstances, act as an amplifier [7]. Vortex structures can also create unsteady heat release rate as a result of a collision with a boundary. This collision will cause sudden ignition of the vortex, generating a heat release pulse. A significant amount of experimental analysis has been

performed in recent years in various geometries and operating conditions to analyze combustion instabilities in the context of flame-vortex interactions. However, theoretical work on this subject is mostly numerical. Analytical models examining the effects of the unsteady flow on the flame should be developed.

### 1.2.3 Equivalence Ratio Fluctuations (Mixture Inhomogeneities)

Several theoretical and experimental studies reveals that equivalence ratio oscillations are important source of combustion instabilities [53, 54, 55, 56]. Both the oscillations in fuel and oxidizer flow rates result in equivalence ratio fluctuations. The pressure oscillations in the combustor interact with the fuel supply line, leads to noticeable oscillations in the fuel flow rate. Also, the velocity oscillations at the fuel supply modulates the oxidizer flow rate. From the definition of equivalence ratio, the following equation can be derived, showing the mechanism for the formation of  $\phi$  oscillations:

$$\frac{\phi'}{\bar{\phi}} = \frac{\frac{m'_f}{\bar{m}_f} - \frac{m'_o}{\bar{m}_o}}{1 + \frac{m'_o}{\bar{m}_o}} \quad (1.22)$$

where the subscripts  $f$  and  $o$  denote fuel and oxidizer, respectively and  $m$  is the mass flow rate. The  $\phi$  oscillations formed at the fuel injector convect through the flame zone where it directly effects the burning speed of reactants and the heat of reaction of the mixture causing heat release rate oscillations.

Peracchio et al. [55] developed a nonlinear model to describe the response of a flame to the equivalence ratio oscillations. They utilized a nonlinear relationship relating the heat release rate per unit mass of the mixture to the instantaneous equivalence ratio. Their model extended the previously published flame dynamic and acoustic analyses to include the effects of varying fuel-air ratio induced by the acoustic field. However, limited experimental evidence was available to validate their results.

Lieuwen et al. [56] developed a simple theoretical model to investigate the impact of equivalence ratio oscillations on the stability characteristics of the system. They considered the time evolution of various processes to understand the mechanism responsible from combustion in-

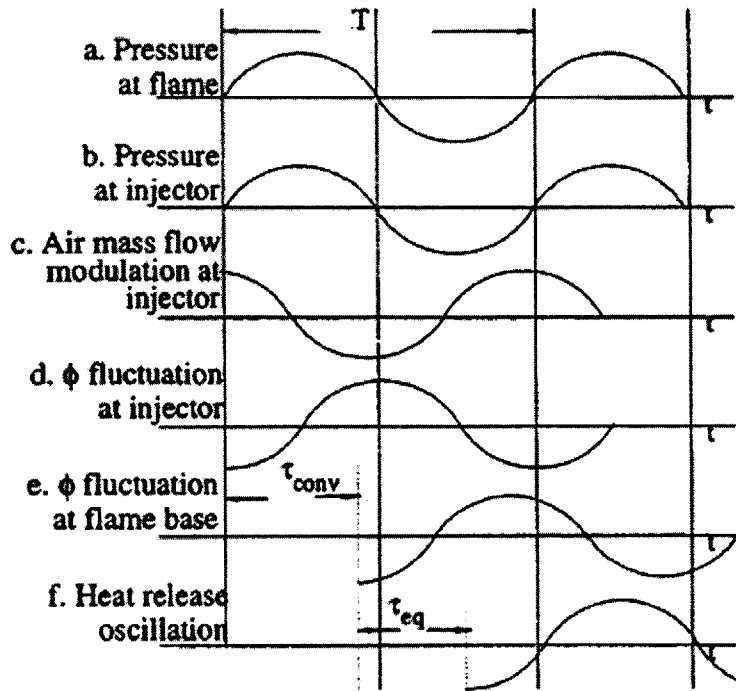


Figure 1-13: Schematic showing the time evolution of disturbances responsible for a combustion instability. From Ref. [56]

stabilities (see Fig. 1-13). Figure (1-13a) shows the time dependent acoustic pressure at the flame with a period  $T$ , assuming compact combustion zone with respect to the wavelength. This disturbance propagates upstream into the inlet duct and produces pressure oscillations at the fuel injector. Without pressure nodes existing between the flame zone and the fuel injector, the pressure disturbances in the flame and the injector are nearly in phase as shown in Fig. (1-13b). The pressure oscillations are accompanied by velocity oscillations which cause fluctuation in the oxidizer mass flow rate. The phase between the pressure and velocity oscillations are determined by the inlet boundary conditions. In Fig. (1-13c), the upstream boundary is assumed to be a pressure node, therefore the velocity leads the pressure by 90 degree. For low Mach number flows, the velocity and the mass flow rate can be assumed to be nearly in phase. Assuming choked fuel injector, i.e.  $m'_f = 0$ , and small oscillations, eqn. (1.22) shows that the equivalence ratio oscillations near the fuel injector are out of phase with the oxidizer flow rate. This is shown in Fig. (1-13d). The reactive mixture with a periodically varying  $\phi$  is convected from the fuel injector to the flame base after a convective time  $\tau_{convect}$ , see Fig. (1-13e). This convective time

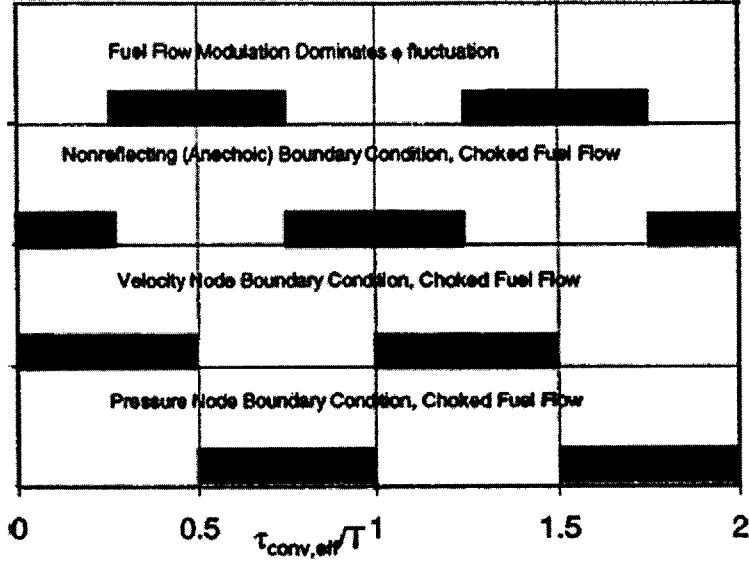


Figure 1-14: Dependence of instability regions (hatched regions) upon  $\tau_{conv,eff}/T$  for several different combustor configurations. From Ref. [56]

can be approximated as:

$$\tau_{convect} \sim \frac{L_{convect}}{U} \quad (1.23)$$

where  $L_{convect}$  is the distance between the flame base and the fuel injector and  $U$  is the mean flow velocity. The reactive mixture reaching the flame zone is not consumed instantaneously, because the different parts of the flow entering the combustor are consumed at different locations of the flame surface. Thus, the total heat release rate lags the  $\phi$  oscillation at the flame base by a time  $\tau_{eq}$ . From Rayleigh's criterion, combustion instability occurs if the pressure is in phase with the heat release rate oscillations; that is, if:

$$\frac{\tau_{convect} + \tau_{eq}}{T} = C_n = n - 1/4 \quad (1.24)$$

where  $n=1,2 \dots$  and  $C_n$  is a constant that depends on the combustor configuration. Thus, the instability regions are primarily a function of  $(\tau_{convect} + \tau_{eq})/T$ , which is denoted as  $\tau_{conv,eff}/T$ . In a combustion system without damping, the instability regions lie in bands where  $C_n - 1/4 < \tau_{conv,eff}/T < C_n + 1/4$ . Figure (1-14) shows the instability bands for different combustor configurations. A relation between  $\tau_{conv,eff}$  and  $\tau_{convect}$  is derived by defining a flame length correction

coefficient,  $\alpha$ :

$$\frac{\tau_{conv,eff}}{T} = \frac{\tau_{convect}}{T} \left(1 + \alpha \frac{L_{flame}}{L_{convect}}\right) \quad (1.25)$$

where  $L_{flame}$  is the length of the flame and  $\alpha \sim 0.5$  for typical combustors. During a combustor operation it can be difficult to determine  $\tau_{conv,eff}/T$  because of its dependence on the length and structure of the flame region. Therefore, to compare the predictions of this model with experimental data,  $\tau_{convect}/T$  is used. In general, the unstable bands predicted by this theory match well with the experimental data. Some small discrepancies can be explained by using  $\tau_{convect}$  instead of  $\tau_{conv,eff}$  for comparisons. However, for some cases significant mismatch between the predictions and experimental data suggests the importance of other instability mechanisms such as flame-vortex interactions.

In the previously mentioned study the  $\phi$  oscillations at the flame base is related to the heat release oscillations by simply shifting the former with  $\tau_{eq}$ . Assuming a quasi-steady relationship between equivalence ratio oscillations and flame speed, Lieuwen [13] described the transfer function relating the  $\phi$  oscillations at the flame base and heat release rate oscillations as follows:

$$\frac{Q'_\phi(t)}{\bar{Q}} = n_H \phi'_b(t - \tau_H) + n_S \frac{d\phi'_b(t)}{dt} \quad (1.26)$$

where  $n_H = \frac{d(\Delta h_R/\Delta \bar{h}_R)}{d\phi}|_{\bar{\phi}}$ ,  $n_S = \tau_H \frac{d(S_u/\bar{s}_u)}{d\phi}|_{\bar{\phi}}$  and  $\tau_H$  can be approximated by  $\tau_H = \frac{L_F}{3\bar{u}}$ . Therefore, the heat release rate oscillations are due to the combined effect of a convective term,  $\tau_H$ , and temporal rate of change of flame speed perturbations. To quantify the dependence of the heat of reaction and flame speed on equivalence ratio, the following correlations from Abu-Off et al. [57] for methane at 300 K and atmospheric pressure can be used:

$$S_u(\phi) = A\phi_B e^{-C(\phi-D)^2} \quad (1.27)$$

$$\Delta h_R(\phi) = \frac{2.9125 \times 10^6 \min(1, \phi)}{1 + \phi 0.05825} \quad (1.28)$$

where  $A = 0.6079$ ,  $B = -2.554$ ,  $C = 7.31$  and  $D = 1.230$ . Figure (1-15) shows the phase and magnitude of the transfer functions relating heat release rate oscillations to equivalence ratio oscillations for different mean equivalence ratios using the given correlations. It is observed that,

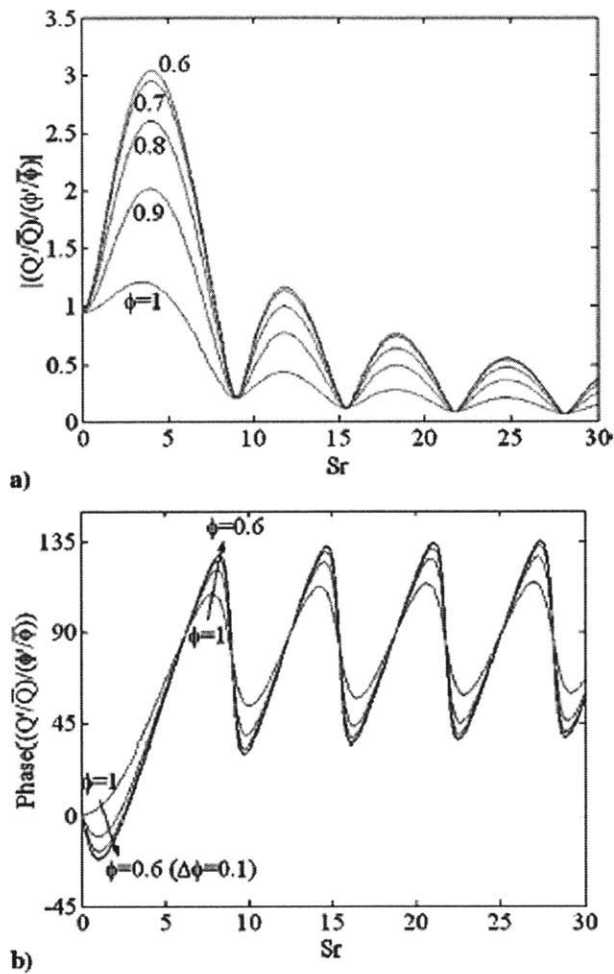


**Figure 1-15: Transfer function magnitude and phase upon Strouhal number From Ref. [13]**

as the mixture becomes leaner, the magnitude of the transfer function increases since the flame speed becomes more sensitive to equivalence ratio oscillation for leaner mixtures. The negative phase values for small Strouhal numbers suggest that a simple convective model ( $n - \tau$ ) is not sufficient to predict the heat release rate oscillations.

Equivalence ratio oscillations are significantly effected by the intensity of mixing taking place between the injector and the flame. If the turbulent mixing process is efficient, the initial level of fluctuations forming in the fuel injector will be diminished to a great extent as the oscillations convect through the flame, thereby causing negligible heat release rate oscillations. Park [58] performed an experimental study in a dumb combustor where he changed the distance between

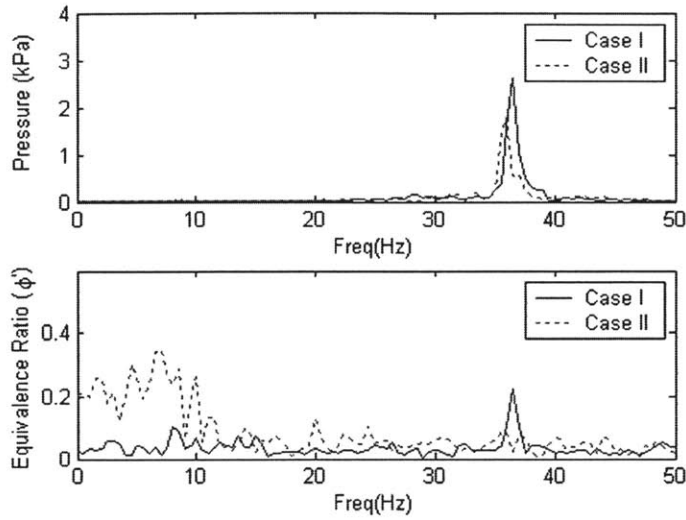


Figure 1-16: Pressure and equivalence ratio frequency spectra at  $Re=5300$  and  $\phi=0.85$  and in cases I and II. From Ref. [58]

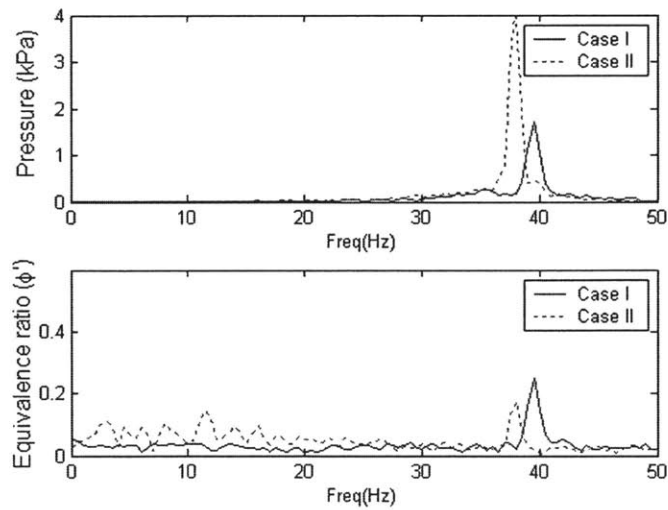


Figure 1-17: Pressure and equivalence ratio frequency spectra at  $Re=8500$  and  $\phi=0.65$  and in cases I and II. From Ref. [58]

the fuel bar and the step (Case I=175 mm and Case II= 300 mm) and the Reynolds number of the main flow in order to investigate the stability characteristics of the combustor. For lower Reynolds number operation, i.e.  $Re = 5300$ ,  $\bar{\phi} = 0.85$ , when the distance was 175 mm, he observed equivalence ratio oscillations at unstable frequency near the flame base. However, when he increased the distance to 300 mm, he did not observe a peak in the equivalence ratio spectrum, suggesting that the  $\phi$  oscillations diminished as they convected through that longer distance. When the main Reynolds number was increased, i.e.  $Re = 8500$   $\bar{\phi} = 0.65$ , he observed equivalence ratio oscillations at the unstable frequency at both distances. Because, at high Reynolds number, the magnitude of the  $\phi$  oscillations formed at the fuel injector are higher and less time is required for the convection from the fuel bar to the flame base compared to the lower Reynolds number case. These observations are shown in Figs. (1-16) and (1-17).

He also used the same stability analysis as Lieuwen et al. [56] which is described above. For  $Re = 8500$  case, both for Cases I and II, the operating conditions correspond to a stable band where equivalence ratio oscillations may damp out pressure oscillations. However, in both cases still significant pressure oscillations were observed. Together with this observation and the vortex shedding mechanism observed from the flame images at the unstable frequency suggested that the essential mechanism of instability was the flame-vortex interactions (see section 1.3.2) not the equivalence ratio oscillations.

#### 1.2.4 Flame-Wall Interactions

A premixed flame interacting with a solid boundary can cause significant heat release rate fluctuations. These fluctuations are induced by rapid rate of change of flame surface area, and they generate an intense sound field. These phenomena are demonstrated in Ref. [59]. A premixed flame is anchored on an axisymmetric burner consisting of a cylindrical tube followed by a convergent nozzle (see Fig. 1-18). A driver unit is used to modulate the upstream flow. Sound measurements are performed when the flame is perturbed at different driving frequencies ( $f_e$ ). Over a wide range of driving frequencies, the sound produced by the system is always 10-20 dB louder than that produced by the same upstream perturbation, but without combustion or



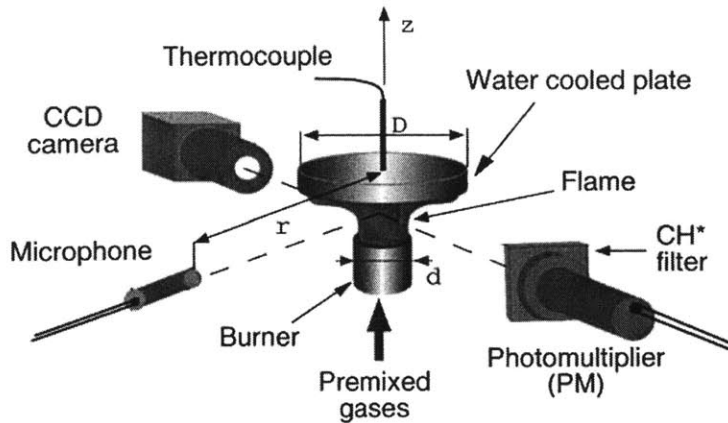


Figure 1-18: Experimental setup. A premixed flame interacts with a plate. From Ref. [59]

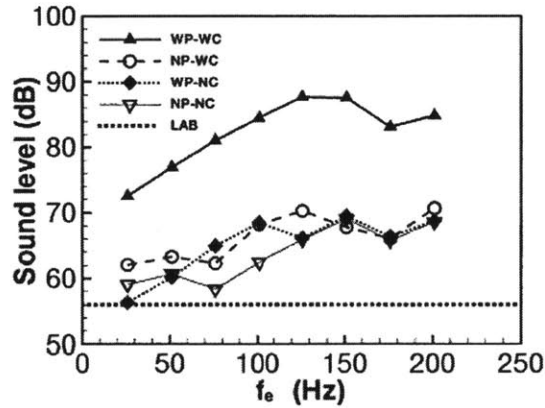
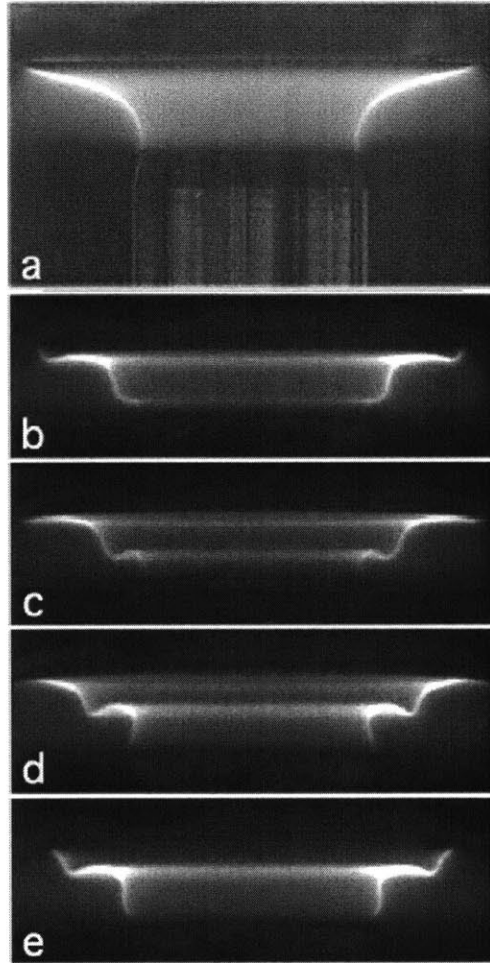


Figure 1-19: Noise measured as a function of driving frequency.  $\bar{u} = 1.44m/s$ ,  $\phi = 0.95$ , burner – platedistance = 7.6mm. WP: with plate, NP: without plate, WC: with combustion, NC: no combustion and LAB: mean background noise in the laboratory. From Ref. [59]

without the plate. This is shown in Fig. (1-19). This study demonstrates that collision of flames with walls in complex situations, such as in a gas turbine combustor, can lead to combustion instabilities.

In Ref. [60], Durox et al. observed self-sustained combustion instabilities of a premixed flame impinging on a flat plate. The flame shape that they observed corresponds to the cool central core geometry observed by Zhang et al. [61]. Figure (1-20a) shows the flame in a steady situation when no sound emission is observed. Figures (1-20b-e) show a typical cycle of oscillations when the instability is triggered. The flame is undulated regularly by a perturbation which leaves the



**Figure 1-20: Different views of the flame: a)Steady-state, and b-e)instantaneous images of the flame during an instability cycle. From Ref. [60]**

burner rim and travels along the front to reach the plate after a certain time delay.

They also developed an analytical model to describe the resonant feedback resulting from the combination of the flame interaction with the plate and with burner acoustics. Their observations indicate that the burner behave like a Helmholtz resonator with a resonance frequency of 200 Hz. The system was modeled by the following equation (details can be found in Ref. [60]):

$$\frac{d^2 v'_1}{dt^2} + 2\delta \frac{dv'_1}{dt} + w_o^2 v'_1 = -N \frac{d^2 v'_1}{dt^2} \Big|_{t-\tau} \quad (1.29)$$

where  $v'_1$  is the velocity oscillation at the burner outlet,  $\delta = \frac{R}{2M}$  is the damping coefficient,

$N = A_1 K(r_{21})n/M$  is a normalized interaction coefficient, and  $\tau = \tau_{21} + \tau_c$  is a global time delay. All the unknown constants are defined in Ref. [60]. Therefore, the dynamics and the stability of the system are described by a second-order equation with delay. It was shown that this model correctly predicted the phase relations between the signals and reproduced the experimental shift in the frequency, which was observed when the burner-to-plate distance was varied.

This study confirms the mechanism by which the interaction of a premixed flame with a wall generates significant surface area fluctuations, which in turn generates an intense pressure field.

### 1.2.5 Unsteady Stretch Rate

Flames usually exist in flow fields which are nonuniform and unsteady. Therefore, it is reasonable to expect that, several flame responses, such as the burning rate and the flame thickness can be effected by the stretch rate. The influence of stretch on the flame response can be discussed based on the normal and tangential components of the flow field at the flame [62]. The tangential velocity gradient at the flame changes the flame surface area  $A$ , and consequently the volumetric burning rate. Through the interaction with heat and mass diffusion, it can also modify the species gradient at the flame, which is related to the reaction rate. The role of the normal velocity gradient is to allow adjustment of the location in the normal direction so that the flame situates where the local flame speed balances the local normal velocity. The G-equation (see eqn. 1.13) describes the dynamics and geometry of the flame surface through the knowledge of the flow velocity at the flame surface, the flame propagation velocity and the geometry of the flame through its unit normal vector. A general definition of stretch at any point on the flame surface is the Lagrangian time derivative of the area  $A$  of an infinitesimal element of the surface is given by:

$$\kappa = \frac{1}{A} \frac{dA}{dt} \quad (1.30)$$

having a unit of  $s^{-1}$ . In terms of the flame propagation velocity,  $S_u$ , the local flow velocity,  $\mathbf{v}$ , and the local radius of curvature,  $\mathfrak{R}$ ,  $\kappa$  can be expressed as [63]:

$$\kappa = \nabla_{\mathbf{t}} \cdot \mathbf{v} - \frac{S_u}{\mathfrak{R}} \quad (1.31)$$

where  $\nabla_t$  is the tangential gradient operator. The first and second terms in the right hand side of equation (1.31) show the effects of aerodynamic straining, and the local flame curvature on the stretch rate, respectively. In the limit of low stretch, Clavin and Joulin [64] showed that the displacement speed is a linear function of stretch rate :

$$\frac{S_u}{S_L} = 1 - \frac{\ell}{S_L} \kappa \quad (1.32)$$

where  $S_L$  is the laminar flame speed,  $S_u$  is the flame propagation speed with respect to the unburned gas and  $\ell$  is a characteristic length that depends on the thermal and diffusive properties of the combustion. The ratio  $\frac{\ell}{d}$ , where  $d$  is a characteristic flame thickness, is called the Markstein number. Substituting eqn. (1.32) in eqn. (1.31), one gets the relation between flame propagation speed and local curvature and strain rate as follows:

$$\frac{S_u}{S_L} = \frac{1 - (\ell/S_L)c\nabla_t \cdot \mathbf{v}}{1 - (c\ell/\mathcal{R})} \quad (1.33)$$

where  $c$  is a correction factor in the order of unity accounting for possible errors when eqn. (1.32) is extended for high stretch values. When integrated over the flame surface, this equation shows that the average strain rate and the flame curvature cause variation in the flame propagation speed, which varies the mass flow rate of the fresh reactants consumed by the flame, therefore the heat release rate.

The flame response to stretch rate has been studied extensively in turbulent combustion for various fuels [65, 66, 67]. Also, several studies have been performed to investigate the response of the flames to external strain rate modulations [68, 69]. Figure (1-21) shows the effect of the strain rate modulation on a stoichiometric methane air flame. It is observed that for low frequency oscillations, the flame translates readily and exhibits large movements causing heat release rate oscillations. However, for high frequency oscillation, its movement is considerably restrained. Since a premixed flame can freely adjust its location in response to changes in the flow, when there is enough time to achieve relocation as in the low frequency forcing case, the flame responds strongly. For high frequencies, the flame does not have enough time to adjust to the changes in the flow field and therefore responds very weakly.

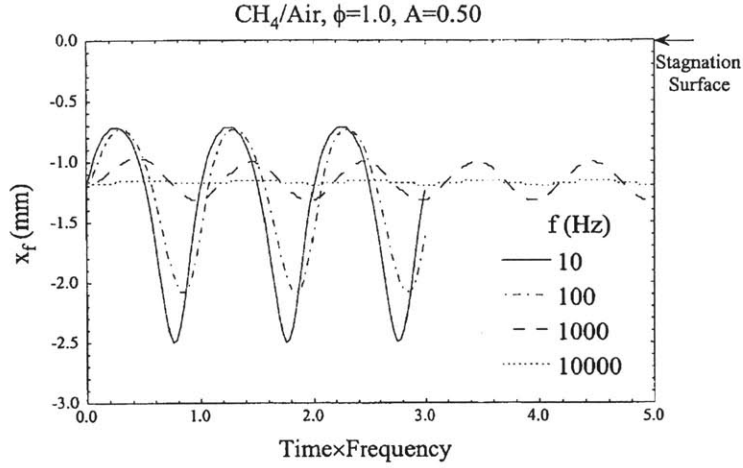


**Figure 1-21: Location of an oscillated methane/air flame, showing the reduced response with increasing frequency. From Ref. [62]**

Another way of demonstrating the effect of strain rate modulations on heat release rate is considering the model equation for flame surface density which is extensively used in turbulent combustion [70]:

$$\frac{d\Sigma}{dt} = \epsilon\Sigma - \beta\Sigma^2 \quad (1.34)$$

In this expression, the first term in the right hand side represents the production of surface density by strain rate, the second shows the mutual annihilation of flame surface density. At equilibrium,  $\epsilon_o\Sigma_o - \beta\Sigma_o^2 = 0$ . A sinusoidal perturbation of the strain rate:  $\epsilon = \epsilon_o + \epsilon_1\cos\omega t$  produces a perturbation in the flame surface density  $\Sigma = \Sigma_o + \Sigma_1$ . Substituting this expression into equation (1.34) and only retaining first order terms in perturbation, one obtains:

$$\frac{d\Sigma_1}{dt} + \epsilon_o\Sigma_1 = (\epsilon_1\cos\omega t)\Sigma_o \quad (1.35)$$

The steady state solution becomes:

$$\frac{\Sigma_1}{\Sigma_o} = \frac{\epsilon_1}{(\epsilon_o^2 + \omega^2)}(\epsilon_o\cos\omega t + \omega\sin\omega t) \quad (1.36)$$

For the low-frequency limit,  $\omega \ll \epsilon_o$ , the relative perturbation of flame surface density is in

phase with the strain rate:

$$\frac{\Sigma_1}{\Sigma_o} = \left(\frac{\epsilon_1}{\epsilon_o}\right)\cos\omega t \quad (1.37)$$

For the high frequency limit,  $\omega \gg \epsilon_o$ , the relative perturbation of flame surface density is out of phase with the strain rate:

$$\frac{\Sigma_1}{\Sigma_o} = \left(\frac{\epsilon_1}{\omega}\right)\sin\omega t \quad (1.38)$$

This analysis again shows that the amplitude of surface density oscillations, i.e, heat release rate oscillations, decreases with the frequency.

### 1.3 Summary

Prediction and control of combustion instabilities is essential for the development of advanced gas turbine combustors and considerable progress has been made in this direction. In general, combustion instabilities, in the form of high amplitude, low frequency oscillations, are observed when the heat release rate oscillations couple positively with the combustor acoustics. Heat release rate oscillations can be formed as a result of acoustic wave-flame interactions, interactions of vortical structures with the flame, equivalence ratio oscillations, flame-wall interactions and unsteady stretch rate. In this chapter all of these mechanisms are reviewed in detail.

Although a lot of information has been accumulated over the past few decades, additional experiments and detailed simulations are still required. Recent experimental studies should be used to verify the results of various combustion dynamic simulations. Enormous physical insight gained about each mechanism should be used as a tool to generate simpler analytical models, especially necessary for control applications.

In the next chapter, a numerical study is performed in order to investigate the flame-vortex interactions in single and double expansion dump combustors.

## Chapter 2

# Numerical Investigation of Flame-Vortex Interactions

In the previous chapter, it was shown that flame-vortex interactions were significant source of combustion instabilities observed in lean premixed combustors (see section 1.2.2). Although many researchers investigated this phenomenon, little was achieved in terms of determining the transfer functions relating the heat release rate and velocity oscillations for the purpose of determining under what conditions the combustor is expected to be stable. Yu et. al. [44] formed a stability criterion for ramjet combustors based on the time scales of acoustic and convective processes. However, they used constant equivalence ratio, therefore did not account for the effects of burning rate on the combustion instability. The objective of this work is to determine the input-output relationship of single and double expansion cavity type dump combustors under various operating conditions. I will investigate under what operating conditions a combustion system is expected to be unstable by considering all the processes that might effect the stability characteristics of the combustor. For this purpose a numerical study is performed to simulate the flame-vortex interaction phenomenon by using the random vortex method. To represent the effect of an acoustic resonance in the reaction region, sinusoidal forcing is imposed on the inlet velocity. A parametric study is performed by varying the forcing frequency and amplitude of the incoming velocity oscillations. Also the laminar burning velocity and the density ratio across the flame is varied to determine the effects of burning rate, i.e. equivalence ratio, on combustion operation.

The study is repeated for a short and a long cavity and different mechanisms responsible from the unsteady heat release rate are reported.

This chapter is organized as follows. In section 2.1, the numerical method is briefly described. Section 2.2 follows with the analysis of the numerical results, where the numerical results are compared with the experimental measurements. The processes responsible for the stability characteristics of both single and double expansion dump combustors are explained by investigating the flame images corresponding to various forcing conditions, flame speeds and density ratios for different cavity lengths, i.e. short cavities and long cavities. In Section 2.3, the chapter is ended with a brief summary.

## 2.1 Numerical Method

In order to examine flame-vortex interactions in a cavity type dump combustor, 2-D numerical simulations are performed using the random vortex method. In this method, the vorticity field is discretized into a finite number of vortex elements, generated at the walls to satisfy no-slip, and advected and diffused in the flow field according to the vorticity transport equation given as:

$$\frac{D\omega}{Dt} = \frac{1}{Re} \nabla^2 \omega \quad (2.1)$$

where  $\frac{D}{Dt}$  is the substantial derivative,  $\omega$  is the vorticity and  $Re$  is the Reynolds number based on the cavity height. A Lagrangian formulation is employed, whereby advection is expressed in terms of a set of coupled ordinary differential equations, and diffusion is simulated by an appropriate random walk mechanism. As a consequence of the two dimensional assumption, flow instabilities and vortex breakup in the third dimension are not included in the model. Simulations are conducted at relatively low Reynolds numbers and no turbulence models are used. Therefore, I expect to be able to capture only large scale structures and their impact on the flame surface propagation and convolution. Vorticity generation across the flame surface due to pressure gradient-density gradient interaction is also neglected. Previous studies showed that the contribution of the separating shear layer vorticity is much more significant than that



produced by the flame under conditions of interest here.

The combustion model is based on the assumptions of a thin flame front separating reactants and products, both modeled as ideal gases, weak flame stretch ( $K_a < 1$ ) and low Mach number flow. The flame is modeled as a surface of discontinuity between the reactants and products, which is advected by the local flow velocity and propagates normal to itself at a given burning velocity. Numerically, the flame is constructed on a uniform square grid using the SLIC algorithm coupled with the VOF method. The algorithm uses a set of straight line segments on a two-dimensional grid to construct the flame interface. The flame is propagated in advection and burning sub-steps. The advection sub-step involves the motion of the flame at the local flow velocity, the burning sub-step, on the other hand, involves the motion of the flame normal to itself into the reactants at a burning velocity  $S_L$ . The burning velocity is modified according to the local radius of curvature such that

$$S_L = S_L^\circ(1 - \ell/R_F) \quad (2.2)$$

where  $S_L^\circ$  is the burning velocity of a planar flame,  $\ell$  is the Markstein length and  $R_F$  is the local radius of curvature of the flame. The density and temperature fields are uniform within the reactants and the products, with a discontinuity at the flame front. Heat release at the flame front is modeled as a localized expansion of the fluid, which is represented using a discrete set of volume expansion sources along the flame interface.

The combustor model requires the specification of the inlet boundary condition at each time step. In order to represent the effect of acoustic resonance in the combustor region and estimating the transfer function of the combustor, that is the relation between the heat release rate and the characteristics of the velocity fluctuations, the inlet velocity is forced sinusoidally at different amplitudes and frequencies according to

$$u = U + a \sin(2\pi ft) \quad (2.3)$$

where  $u$  is the inlet velocity,  $U$  is the mean inlet velocity,  $a$  is the oscillation amplitude and  $f$  is the forcing frequency.

The formulation and details about the numerical scheme can be found in Ref. [71]. The grid size that is used is selected as  $1/15 \times 1/15$ , i.e. dimension 1 is the height of the step. The dimensionless time step used in updating the vorticity field is selected as 0.025.

## 2.2 Results and Discussions

All the parameters I vary in the code to perform the parametric study of the flame response to imposed velocity oscillations are normalized with respect to the mean inlet velocity,  $U$ , and the step height,  $D$ . The non-dimensional parameters are:

Reynolds number

$$Re = \frac{UD}{\nu_u} \quad (2.4a)$$

Strouhal number

$$St = \frac{fD}{U} \quad (2.4b)$$

Normalized oscillation amplitude

$$a^* = \frac{a}{U} \quad (2.4c)$$

Normalized burning velocity

$$S_u = \frac{S_L}{U} \quad (2.4d)$$

Density ratio across the flame

$$\Lambda = \frac{\rho_u}{\rho_b} \quad (2.4e)$$

Cavity height

$$H^* = \frac{H}{D} \quad (2.4f)$$

Cavity length

$$L^* = \frac{L}{D} \quad (2.4g)$$

where  $\nu_u$  is the kinematic viscosity of the unburned gas,  $f$  is forcing frequency,  $a$  is the oscillation

amplitude of the inlet velocity,  $S_L$  is the laminar burning velocity of the flame,  $\rho_u$  is the density of the unburned gas,  $\rho_b$  is the density of the burned gas,  $H$  is the cavity height and  $L$  is the cavity length.

### 2.2.1 Double expansion dump combustor

I simulated a double expansion dump combustor with short and long cavity lengths,  $L^* = 4$  and  $L^* = 8$ , respectively, and compared the heat release rate dynamics in the two cases. Yu et al. [44] performed experiments in the same geometry and showed that the flame images in the two halves of the combustor were symmetric. Therefore, only one half of the combustor is simulated imposing symmetry along the combustor centerline.

### 2.2.2 Short Cavity

I start by comparing the results, in terms of the flame shapes and heat release dynamics, with those in [44]. For that purpose, the code was run at the similar values for the parameters used in the experiment mentioned in that reference. I set:  $Re = 10,000$ ,  $St = 0.113$ ,  $a^* = 1.3$ ,  $S_u = 0.0125$ ,  $\Lambda = 4$ ,  $H^* = 1.6$  and  $L^* = 4$ . To improve the computational efficiency of the code, Reynolds number used in the simulations is lower than that used in the experiment. I will show later that Reynolds number has a negligible effect on the heat release rate dynamics and flame shape in the range of conditions considered here.

Figure (2-2) shows the heat release rate and velocity in a typical cycle. The flame images shown in Fig. (2-1) are constructed by averaging over several cycles, and the different images correspond to the numbers shown in Fig. (2-2). I start the analysis of these images and the correspondence between the flame shape, the vortex and the heat release rate from the moment of maximum inlet acceleration, according to Fig. (2-2). Around the moment of maximum inlet flow acceleration, fresh reactants are entering the combustor, pushing the flame downstream. The wake vortex starts to form at this point, corresponding to Fig. (2-2), (1). As the velocity increases, the vortex grows and rapidly convects downstream. The flame rolls up around the

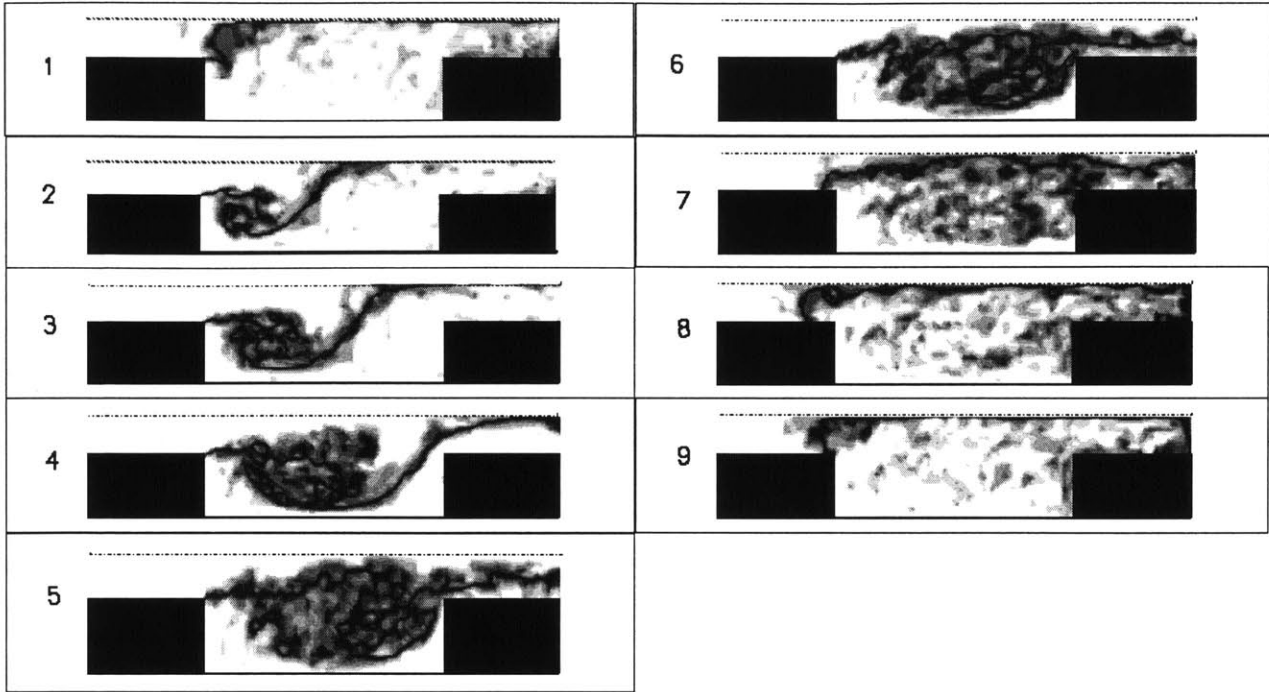


Figure 2-1: Flame images in a typical cycle

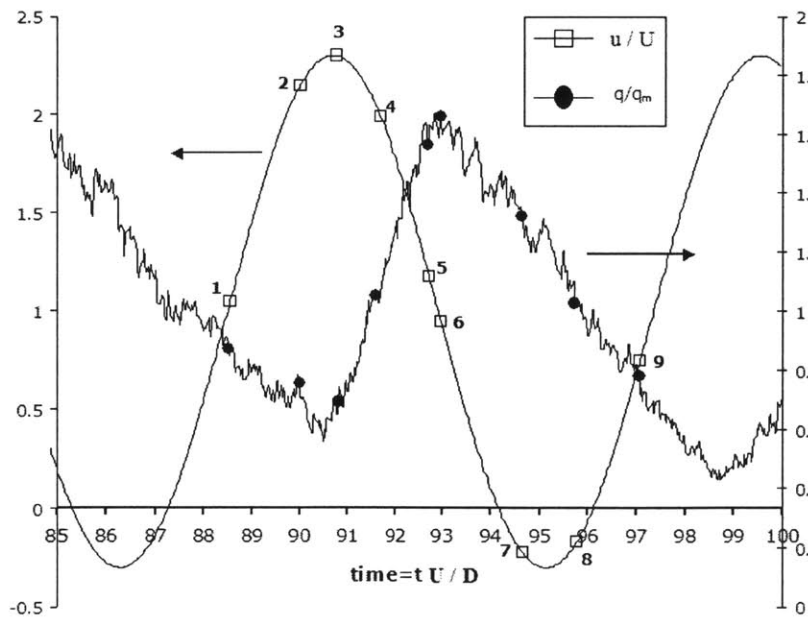


Figure 2-2: Velocity and heat release rate oscillations.  $q_m$  is the average heat release rate. Points correspond to the images in Fig. (2-1)

growing vortex, trapping reactants as it folds, Fig. (2-2), (2)-(3). The heat release rate is minimum around the moment of maximum inlet velocity (3). The fourth image is taken at the moment prior to the impingement of the vortical structure onto the forward facing step of the cavity. The vortex grows further by trapping more reactants within its structure, reaching its maximum size in (5). Between (5)-(6), the leading edge of the vortex impinges on the forward step, the vortex breaks up into smaller structures, allowing for the trapped reactants to burn quickly by the extra flame surface area. At this moment the inlet velocity is still above its mean value. After a short time, while all the trapped reactants within the vortical structure are being consumed, the heat release rate reaches its maximum (6). At this instant the vortex has completely broke up. The minimum velocity occurs between images (7) and (8). Because of flow reversal, the flame moves upstream of the backward facing step. At this moment, the entire combustor is almost filled with products. Following this event, the velocity is again positive, and rising at a steep acceleration. Fresh reactants enter the combustor, forcing the flame to move downstream of the step (9). As the maximum flow acceleration is reached, a new vortex forms at the step and the cycle repeats itself.

The relationship between the heat release rate and the velocity shown in Fig. (2-2) matches closely the experimental data in Ref. [44]. Figure (2-3) shows the flame images obtained in Ref. [44] in a typical unstable cycle. The numbers on the images approximately correspond to the instances in Fig. (2-2). Comparing Figs. (2-1) and (2-3), I conclude that the timings of the events in the numerical simulations and the experimental results match well within the error range of the current study. In the first three images the numerical results slightly lag the experiment because of the small differences in the parameters used. The maximum heat release rate in the experimental data and in the numerical results occurs a short time after the vortex impinges on the forward step, due to the sudden burning of the trapped reactants associated with the break up of the large structure. As suggested by Yu et al., the moment when the leading edge of the vortex collides with the forward facing step is determined by the convective time scale,  $\tau_{conv} = \frac{L}{U}$ . In the simulation, the dimensionless value of this time scale is:

$$\frac{\tau_{conv}U}{D} = \frac{L}{D} = L^* = 4 \quad (2.5)$$

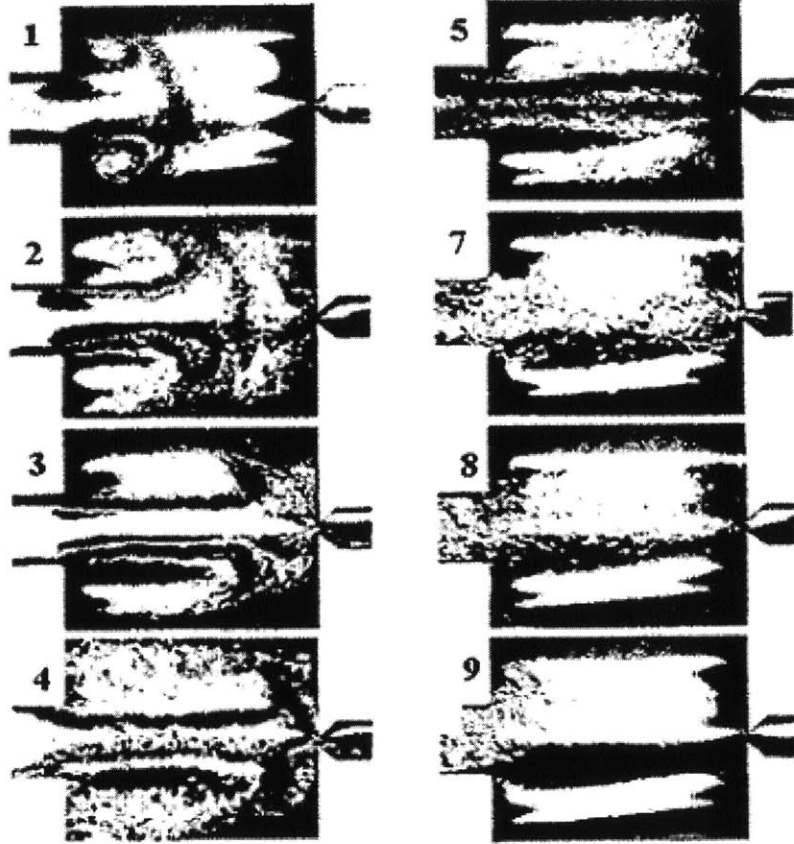
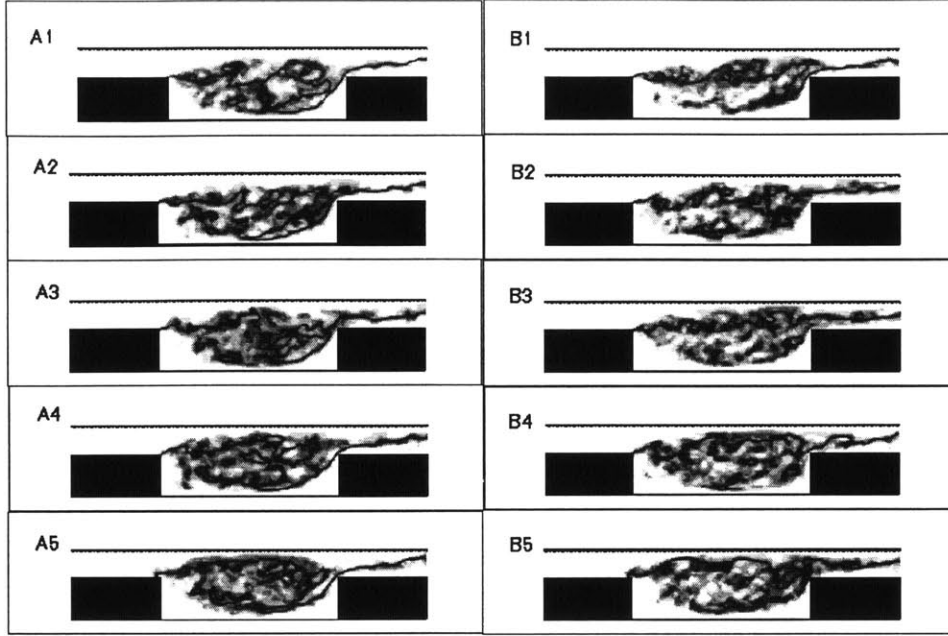


Figure 2-3: Flame images in an unstable cycle from Ref. [44]

which can be easily verified from Fig. (2-2). This agreement between the numerical results and the experimental observations demonstrates the applicability of the model for this problem. Next, I use the same model to perform a more detailed parametric study of the flame response to different input velocity oscillations.

I ran the simulation at different  $St$  and  $S_u$  values, keeping other parameters constant. Figure (2-4) shows the moment in the cycle when  $\frac{\tau_{conv}U}{D} = 4$ . It is seen that regardless of  $S_u$  and  $St$ , this moment corresponds to the instance when the leading edge of the large wake vortex collides with the forward facing step. Examination of the instance of the maximum heat release rate under the conditions shown in Fig. (2-4) reveals that the phase between the instance when the leading edge of the vortex impinges on the forward facing step and the heat release reaches a maximum is dependent on  $S_u$  and  $St$ , with the former having a more significant effect. It is seen



**Figure 2-4:** Flame images at the instance when  $\frac{\tau_{conv}U}{D} = 4$  for various  $St$  and  $S_u$  values. First column (A) and second column (B) correspond to  $S_u=0.0125$  and  $S_u=0.015$ , respectively. From top row(1) to bottom row(5) the figures correspond to  $St$  values, 0.08, 0.095, 0.113, 0.13 and 0.15, respectively

that increasing  $S_u$ , or equivalence ratio, decreases this phase significantly. This is consistent with the fact that the reactants trapped within the vortical structure burn faster at higher  $S_u$ . Next, I use these observations to formulate a simple model to predict the phase between the heat release rate and velocity, i.e. the transfer function phase relating heat release rate to velocity oscillations, as follows:

$$\phi_{q'-u'} = \left( \frac{L}{U} \frac{1}{\tau_{tot}} - \frac{1}{4} \right) 2\pi + \phi_{bur} \quad (2.6)$$

where  $\tau_{tot}$  is the oscillation period and  $\phi_{bur}$  is the phase between the instance when the leading edge of the vortex impinges on the forward facing step and the maximum heat release rate. Values for  $\phi_{bur}$  calculated from the numerical results are shown in Table 1. As seen in Table 1, even a small increase in  $S_u$  decreases  $\phi_{bur}$  significantly because of faster burning of reactants.  $\phi_{bur}$  can simply be modeled as:

$$\phi_{bur} = \frac{V_{trapped}}{A_f S_L} \frac{1}{\tau_{tot}} 2\pi \quad (2.7)$$

where  $V_{trapped}$  is the total volume of trapped reactants and  $A_f$  is the average flame surface area.

**Table 2.1: Phase between the initiation of vortex breakup and maximum heat release rate ( $\phi_{bur}$ ) for various normalized flame velocity ( $S_u$ ) and Strouhal numbers ( $St$ ) calculated from the simulation results**

$\phi_{bur}$ (deg)	$St = 0.08$	$St = 0.095$	$St = 0.113$	$St = 0.13$	$St = 0.15$
$S_u = 0.0125$	69.0	62.7	60.8	60.4	57.2
$S_u = 0.015$	58.3	47.2	39.4	37.1	34.6

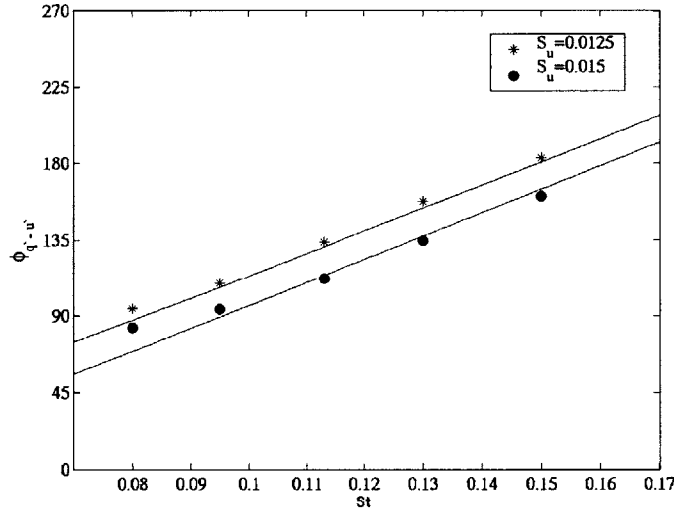


**Figure 2-5:  $\phi_{q'-u'}$  (in degrees) vs  $St$  for different  $S_u$  values. Curves are the predictions of the model in eqn. (2.10)**

With respect to the non-dimensional parameters that we use in our study, eqn. (2.7) becomes:

$$\phi_{bur} = \frac{V_{trapped}^*}{A_f^* S_u} St 2\pi \quad (2.8)$$

where  $V_{trapped}^*$  and  $A_f^*$  are defined as  $\frac{V_{trapped}}{D^3}$  and  $\frac{A_f}{D^2}$ , respectively. Using the values in Table 1, I formed a relation for  $\frac{V_{trapped}^*}{A_f^*}$  as functions of  $St$  and  $S_u$ .  $\phi_{bur}$  becomes:

$$\phi_{bur} = \frac{1}{6302.5 S_u^{1.9} St^{0.2}} \quad (2.9)$$

Substituting eqn. (2.9) into eqn. (2.6) and non-dimensionalizing gives:

$$\phi_{q'-u'} = 2\pi(L^* St - \frac{1}{4}) + \frac{1}{6302.5 S_u^{1.9} St^{0.2}} \quad (2.10)$$



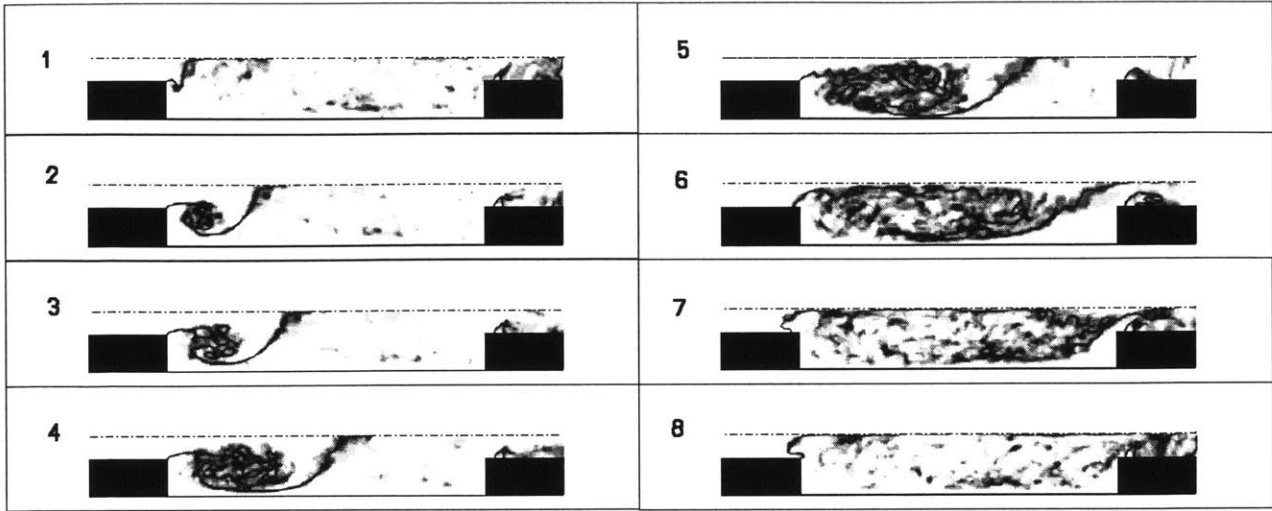


Figure 2-6: Flame images in a typical cycle

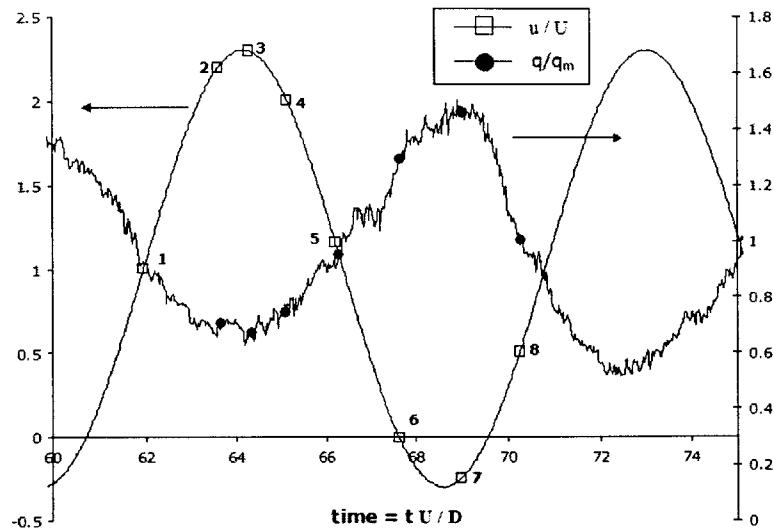
which is valid for  $0.07 \leq St \leq 0.17$  and  $0.01 \leq S_u \leq 0.015$ .

Figure (2-5) shows the phase between the heat release rate and velocity oscillations at a range of  $St$  for two values of  $S_u$ . The curves are predictions of the model in eqn. (2.10) and data points are results from the numerical simulation.

### 2.2.3 Long Cavity

Next, the length of the cavity is doubled to determine the effect of the cavity geometry on the flame-vortex interaction mechanism and its impact on the heat release dynamics. I set:  $Re = 10,000$ ,  $St = 0.113$ ,  $a^* = 1.3$ ,  $S_u = 0.0125$ ,  $\Lambda = 4$ ,  $H^* = 1.6$  and  $L^* = 8$ .

Flame images shown in Fig. (2-6) are obtained by averaging all unstable cycles and closely correspond to the heat release rate and velocity data shown in Fig. (2-7). I start the analysis with the moment of maximum inlet acceleration (1). Similar to the short cavity, fresh reactants enter the combustor with maximum acceleration and the wake vortex starts to form. As the velocity rises, reaching a maximum between (2) and (3), the wake vortex grows while moving downstream. The flame rolls-up into the growing vortex, forming a zone of trapped reactants. Near the moment of maximum velocity the heat release rate is minimum. In the next two images, (4) and (5), the vortex structure continues to grow and heat release rate rises gradually.



**Figure 2-7: Velocity and heat release rate oscillations. Points correspond to the images in Fig. (2-6)**

Following the fifth image the inlet velocity drops below its average, slowing the downstream motion of the vortex, which, in turn, grows more in the cross stream direction. In the sixth image, the inlet velocity is nearly zero, and the vortex impinges on the cavity centerline, i.e. it reaches its maximum size. At this moment the breakup of the vortex followed by formation of small scale structures is ensued. Due to intense burning associated with the formation of small scales, the heat release rate increases rapidly. Image (7) corresponds to the moment of maximum heat release rate when the trapped reactants burn completely. At this instance, the velocity is negative, and the flame moves upstream of the backward facing step. In the last image, (8), the burning rate is very low, the combustor is mostly filled with the combustion products and the heat release rate has dropped significantly from its maximum value. Furthermore, the velocity is recovered and the flow is accelerating. As the moment of maximum inlet acceleration is reached again, fresh reactants enter the combustor. The wake vortex starts forming, and the cycle repeats itself.

Comparing the flame images in the cases of a short and a long cavity, I observe that the mechanisms by which the vorticity breakup is initiated are different. As shown earlier, for the short cavity case, vortex breakup starts as the large wake vortex hits the forward facing step. To the contrary, in the long cavity case, the vortex never reaches that for downstream. Instead,

**Table 2.2: Phase between the initiation of vortex breakup and maximum heat release rate ( $\phi_{bur}$ ) for various normalized flame velocity ( $S_u$ ) and Strouhal numbers ( $St$ ) calculated from the simulation results.  $H^*=1.6$**

$\phi_{bur}$ (deg)	$St = 0.08$	$St = 0.095$	$St = 0.113$	$St = 0.13$	$St = 0.15$
$S_u = 0.0125$	39.5	54.0	63.0	85.9	114.8
$S_u = 0.015$	20.9	28.5	39.9	58.4	78.5

the vortex breakup is initiated as the vortex grows in the cross flow direction and hits the other vortex structure forming on the other side of the centerline.

Now, I generalize my observation for the long cavity by examining the flame images, and the phase between heat release rate and velocity oscillations at different values of  $St$ ,  $S_u$  and  $H^*$ . In all cases, similar behavior as described above is observed, validating the proposed mechanism for the initiation of vortex breakup. Furthermore, the moment of vortex breakup is found to be functions of  $St$  and  $H^*$  and negligibly effected by  $S_u$ . Table 2 shows the phase between the initiation of vortex breakup and the moment of maximum heat release rate, i.e.  $\phi_{bur}$ , for different  $S_u$  and  $St$  values, respectively for  $H^*=1.6$ . It is observed that as  $S_u$  increases  $\phi_{bur}$  decreases, as also observed in the short cavity. This is because of the faster burning of the trapped reactants in the vortex as the equivalence ratio increases. However, unlike the short cavity,  $\phi_{bur}$  shows strong dependence on  $St$ , i.e. forcing frequency. Forming a simple analogy with the short cavity, the phase between the heat release rate and velocity oscillations can be expressed as:

$$\phi_{q'-u'} = 2\pi(aH^{*b}St^c - \frac{1}{4}) + \frac{1}{dS_u^eSt^f} \quad (2.11)$$

The first term gives the phase between the maximum inlet velocity and the moment when the the vortex reaches the centerline, i.e. when vortex breakup is initiated, and the second term is the phase between the moment of maximum heat release rate and the initiation of vortex breakup, i.e.  $\phi_{bur}$ .  $a$ ,  $b$ ,  $c$ ,  $d$  and  $e$  are constants which are determined by curve fitting. Their values are:  $a=0.9205$ ,  $b=1.1$ ,  $c=0.4677$ ,  $d=57.875$ ,  $e=1.9$  and  $f=-1.9$ . This model is valid for:  $0.07 \leq St \leq 0.17$ ,  $0.01 \leq S_u \leq 0.015$  and  $1.5 \leq H^* \leq 2$ .

Figure (2-8) shows the phase between the heat release rate and velocity oscillations as a function of  $St$  for different  $S_u$  values. Comparing to the short cavity, the phase is larger and the

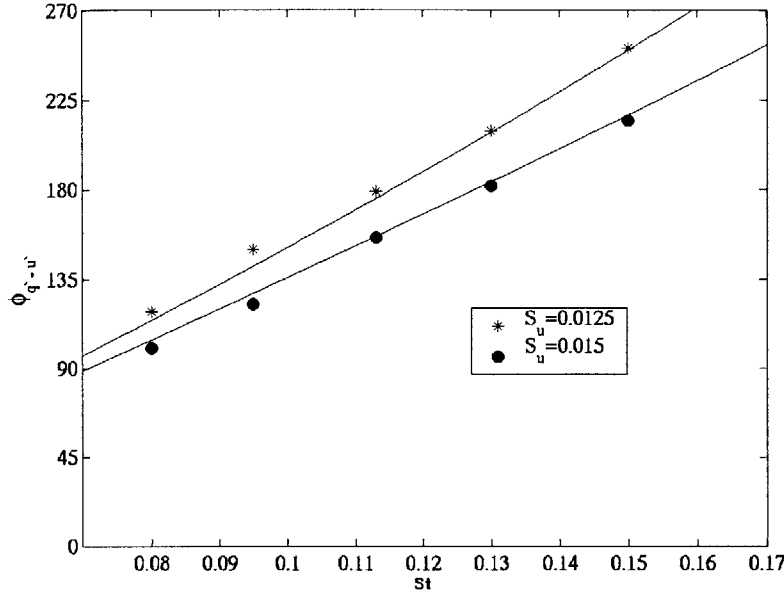


**Figure 2-8:**  $\phi_{q'-u'}$  (in degrees) vs  $St$  for different  $S_u$  values. Curves are the predictions of the model in eqn. (2.11)

slope of the lines are higher. The phase is larger because more time is needed for the initiation of the vortex breakup. A higher slope implies that  $St$  has more effect on the phase compared to the short cavity case. Also, as  $S_u$  increases, the phase decreases due to the faster burning of the trapped reactants within the vortical structure, which is also observed in the short cavity.

I have observed two distinct mechanisms for the initiation of vortex breakup for a short cavity and a long cavity. A criterion is required to be defined to decide which mechanism is expected under given operating condition defined by  $St$ , and cavity geometry. Defining the ratio:

$$r = \frac{L^*}{0.9205H^{*1.1}St^{-0.5323}} \quad (2.12)$$

The numerator and denominator of eqn. (2.12) are the time scales for initiation of vortex breakup for short and long cavities, respectively. If  $r < 1$ , the mechanism of vortex breakup is controlled by the impinging of the wake vortex to the forward facing step, and the combustor is considered as a short cavity one. Conversely, if  $r > 1$ , the mechanism of vortex breakup is controlled by impinging of the wake vortex to the vortex structures forming in the other side of the centerline,

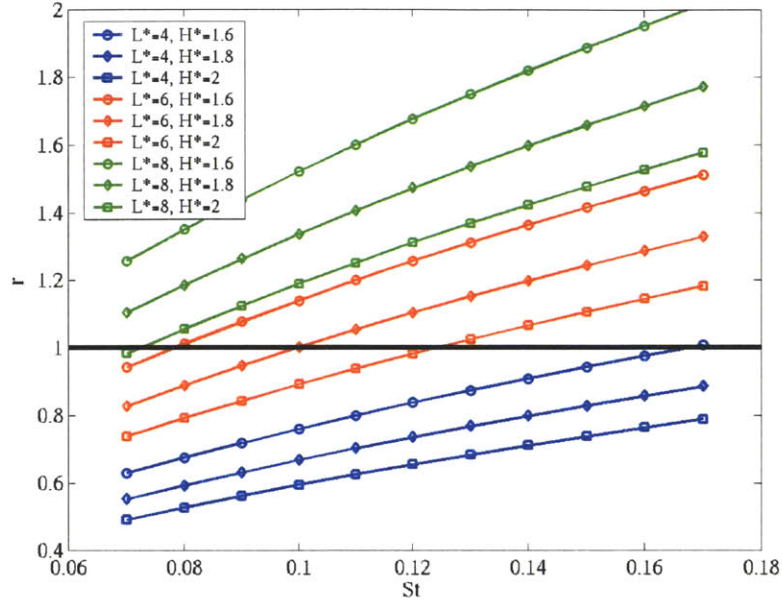


Figure 2-9:  $r$  vs  $St$  for for various cavity geometries

and the combustor is considered as a long cavity one.

Figure (2-9) shows ratio  $r$  at a range of  $St$  for various cavity geometries. I observed that for some cavity geometries defined by  $L^*$  and  $H^*$ , e.g.  $L^*=6$  and  $H^*=1.8$ , whether the combustor behaves as a short or a long cavity one is determined by  $St$ .

## 2.2.4 Single expansion dump combustor

Finally, a parametric study in a single-expansion dump combustor is performed. In this section I also investigate the effect of Reynolds number,  $Re$ , oscillation amplitude,  $a^*$ , and density ratio,  $\Lambda$ , in addition to  $S_u$  and  $St$  on the heat release dynamics. I fix the geometry of the combustor at the values  $L^* = 8$  and  $H^* = 2$ . For this case, the upper wall acts as a no-slip boundary condition. First, I investigate the effect of Reynolds number on the heat release rate by running the simulation while varying Reynolds number for a range of Strouhal numbers.  $S_u$ ,  $\Lambda$  and  $a^*$  are kept constant at the values 0.02, 3 and 1.3, respectively. Figure (2-10) shows the phase between the heat release rate and velocity oscillations,  $\phi_{q'-u'}$ , as a function of the Strouhal number for

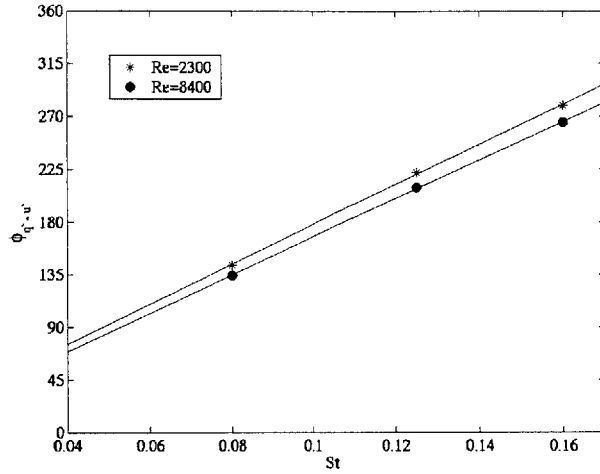


**Figure 2-10:**  $\phi_{q'-u'}$  (in degrees) vs  $St$  for  $Re=2300$  and  $8400$  at constant  $S_u$  and density ratio

Reynolds numbers 2300 and 8400. It is observed that as Reynolds number increases, the phase between velocity and heat release rate oscillations decreases slightly (about  $10^\circ$  as  $Re$  increases to 8400 from 2300), which is a negligible change for the purpose of the study considering that Reynolds number is more than tripled.

Now, while fixing the Reynolds number and the geometry of the combustor, I investigate the phase between heat release rate and velocity oscillations by varying  $St$ ,  $S_u$ ,  $a^*$  and  $\Lambda$ . Figures (2-11) and (2-12) show the phase,  $\phi_{q'-u'}$ , as a function of the Strouhal number for various  $S_u$  and  $\Lambda$  values for  $a^* = 1.3$  and  $1.1$ , respectively. To give a better sense of the parameters used in generating these figures, for propane with  $U = 6m/s$ , the equivalence ratio range  $0.57 - 0.8$  approximately corresponds to  $S_u$  range  $0.02 - 0.04$  and density ratio range  $5.8 - 7.1$ .

Comparing these figures, I conclude that the forcing amplitude,  $a^*$ , has a negligible effect on the phase between velocity and heat release rate oscillations. Small differences in the two figures, i.e.  $\sim 5-10$  deg., are in the error range of the current study. Increasing  $S_u$  and density ratio, shifts the lines towards lower phase values due to increased burning rate.

Examining the flame images corresponding to the data points in Fig. (2-11), a similar mechanism as in the long cavity double expansion dump combustors is observed. However, for this geometry, especially for low Strouhal numbers, significant amount of reactants escape from the

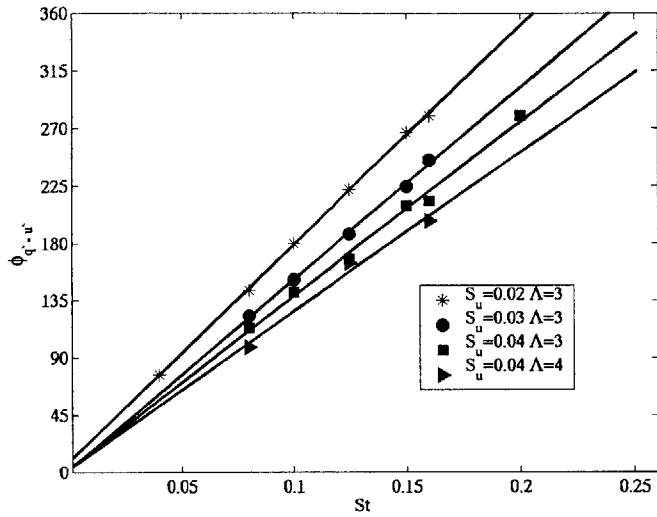


Figure 2-11:  $\phi_{q'-u'}$  (in degrees) vs  $St$  for various  $S_u$  and density ratios. Amplitude of oscillations is 1.3. Straight lines are linear fits

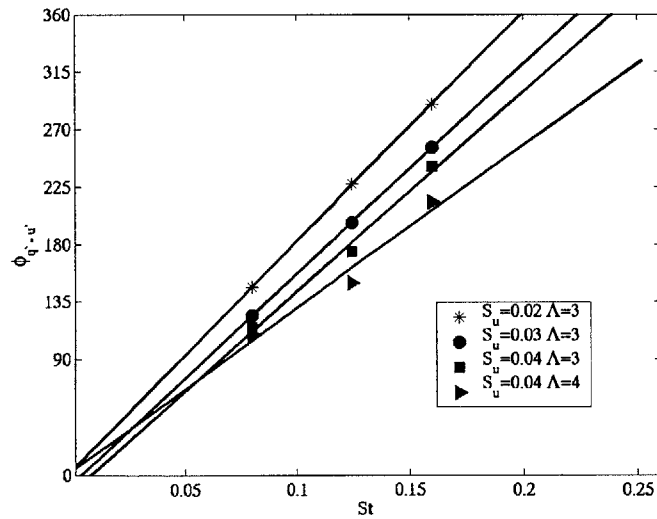
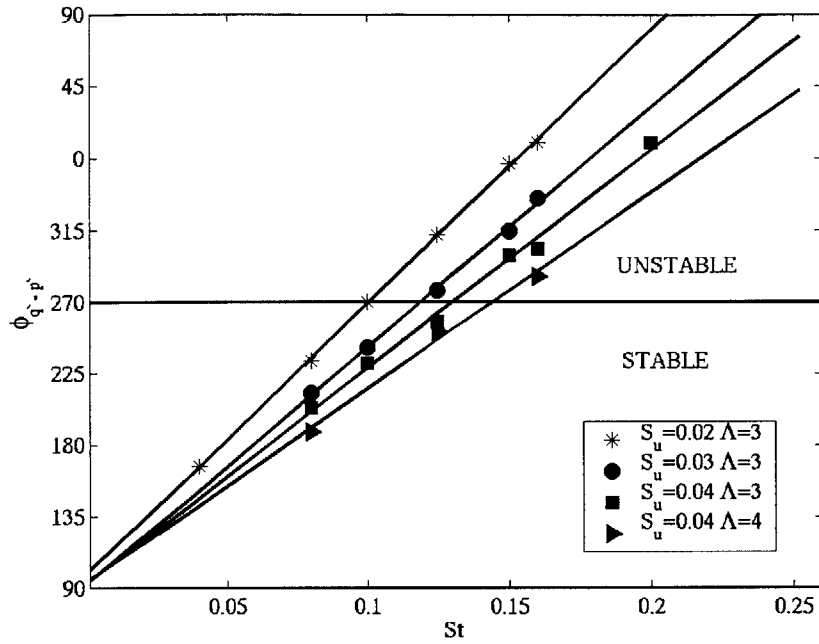


Figure 2-12:  $\phi_{q'-u'}$  (in degrees) vs  $St$  for various  $S_u$  and density ratios. Amplitude of oscillations is 1.1. Straight lines are the linear fits



**Figure 2-13:**  $\phi_{q'-p'}$  (in degrees) vs  $St$  for various  $S_u$  and density ratios.  $a^*=1.3$ . Data points are numerical results. Straight lines are linear fits.

combustor, making the role of the forward facing step more significant. In the beginning of a cycle the vortex forms and convects downstream. The flame rolls up into the growing vortex. As the velocity drops from its maximum value, the vortex starts to grow in the cross stream direction, hitting the upper wall and initiating the vortex breakup. (It is known that depending on  $St$  and combustor geometry vortex breakup can also be initiated when the vortex hits the forward facing step). A short time after this, the reactants trapped inside the vortical structure burn and the maximum heat release rate is reached. The time between the initiation of the vortex breakup and the maximum heat release depends on the operating conditions, i.e.  $S_u$ ,  $\Lambda$  and  $St$ . As the inlet velocity becomes negative, the flame moves upstream of the backward facing step. Near the end of the cycle, velocity recovers and new reactants are admitted into the combustor. The new cycle begins as the vortex structure again begins to form. Similar mechanism is observed in an experimental study by Ghoniem et al. [72] in a backward-facing step dump combustor. Intense burning in the combustor as a result of vortex breakdown occurred after the flame reached the upper wall of the cavity.



In order to determine under what conditions the combustor operation is expected to be stable or unstable we need to determine the phase between heat release rate and pressure oscillations,  $\phi_{q'-p'}$ . Using Rayleigh's criterion, the combustor is unstable when:

$$N - \frac{1}{4} < \frac{\phi_{q'-p'}}{2\pi} < N + \frac{1}{4} \quad (2.13)$$

where  $N$  is an integer. In Fig. (2-13), I plot the transfer function phase,  $\phi_{q'-p'}$ , relating the heat release rate and pressure oscillations as a function of  $St$  for the cases shown in Fig. (2-11), while assuming quarter wave mode between pressure and velocity oscillations, as observed in [72]. It is seen from the figure that at constant  $S_u$  and  $\Lambda$ , the combustor shifts from stable to unstable operation as  $St$  increases above a certain value. Also, as  $S_u$  and density ratio increase the lines shift through the stable operating band near  $St=O(0.1)$ . Therefore, at constant  $U$ , increasing the equivalence ratio of the system, or increasing  $S_L$  in lean regime, shifts the system towards stable operating conditions for  $St=O(0.1)$ . However, the same conclusion cannot be reached by keeping the equivalence ratio constant but reducing  $U$ , although this will also increase  $S_u$ . This is because  $St$  is also dependent on the mean flow velocity and decreasing  $U$  increases  $St$ , shifting the system towards the unstable operating band.

## 2.3 Summary

In this chapter, I investigated flame-vortex interaction mechanism in double and single expansion dump combustors under various operating conditions. It was observed that the unsteady interaction of the wake vortex with the flame derived the instability in all cases by governing the heat release dynamics. I showed that for all cases studied, the moment of maximum heat release rate occurred a short time after the breakup of the large wake vortex causing intense burning of the trapped reactants within the vortical structure. For long and short cavities, the mechanism by which the vortex breakup is initiated are different. For short cavities vortex breakup is initiated as the wake vortex moves downstream and hits the forward facing step, the moment of which solely depending on the convective time scale defined as the cavity length divided by the mean velocity. In long cavities, vortex never reaches the forward facing step. Vortex breakup

occurs as the vortex grows in the cross stream direction and hits the upper wall (single expansion dump combustor) or other vortex formed in the other side of the combustor centerline (double expansion dump combustor) which is controlled by the Strouhal number and the combustor geometry. Also, the time between the initiation of vortex breakup and maximum heat release rate is inversely proportional to the burning rate in the combustor. For all the geometries studied, as the burning velocity and the density ratio is increased, the phase decreases because of the higher burning rate in the combustor. By assuming a quarter wave mode between pressure and velocity oscillations I observed that below certain equivalence ratio the operation of the combustor shifted from stable to unstable operating band, which is also observed in various experimental studies. I formed models predicting the transfer function phase relating the heat release rate to velocity oscillations in double expansion dumb combustor, both for short and long cavities at a range of input parameters. Furthermore, performing a parametric study in a single expansion dump combustor, I showed that Reynolds number and the amplitude of inlet velocity oscillation had negligible effects on the transfer function phase at constant burning velocity, density ratio across the flame and Strouhal number.

In the next chapter, the effect of secondary air injection near the dump plane on equivalence ratio oscillations in a backward facing step combustor is investigated.

## Chapter 3

# Effect of the Air Injection in Cross Stream Direction on Equivalence Ratio Oscillations

Air injection in the cross stream direction, close to the dump plane, was shown to improve the stability of a lean premixed backward facing step combustor [73]. Its effect on stability was explained in terms of its effect on the fluid dynamics in the combustor. In this chapter, the effect of the secondary jet on equivalence ratio oscillations is investigated. High amplitude pressure oscillations within the combustor, during unstable operation, may cause fluctuation in the secondary jet velocity. When combined with the incoming equivalence ratio oscillations, this unsteady jet may significantly change the amplitude and phase of the equivalence ratio oscillations reaching the flame depending on the amplitude of the secondary jet and the primary stream oscillations, their relative phase and the momentum ratio of the secondary jet to the primary flow. First, a simple experiment is performed in the MIT backward facing step combustor to validate the proposed mechanism. The velocity of the primary flow and the secondary jet are measured simultaneously in a non-reactive experiment while forcing the flow using a loud speaker. After investigating the mechanism in non-reacting flow experiment, the acoustics of the combustor is modeled to gain further insight into the effect of the secondary jet on the equivalence ratio and

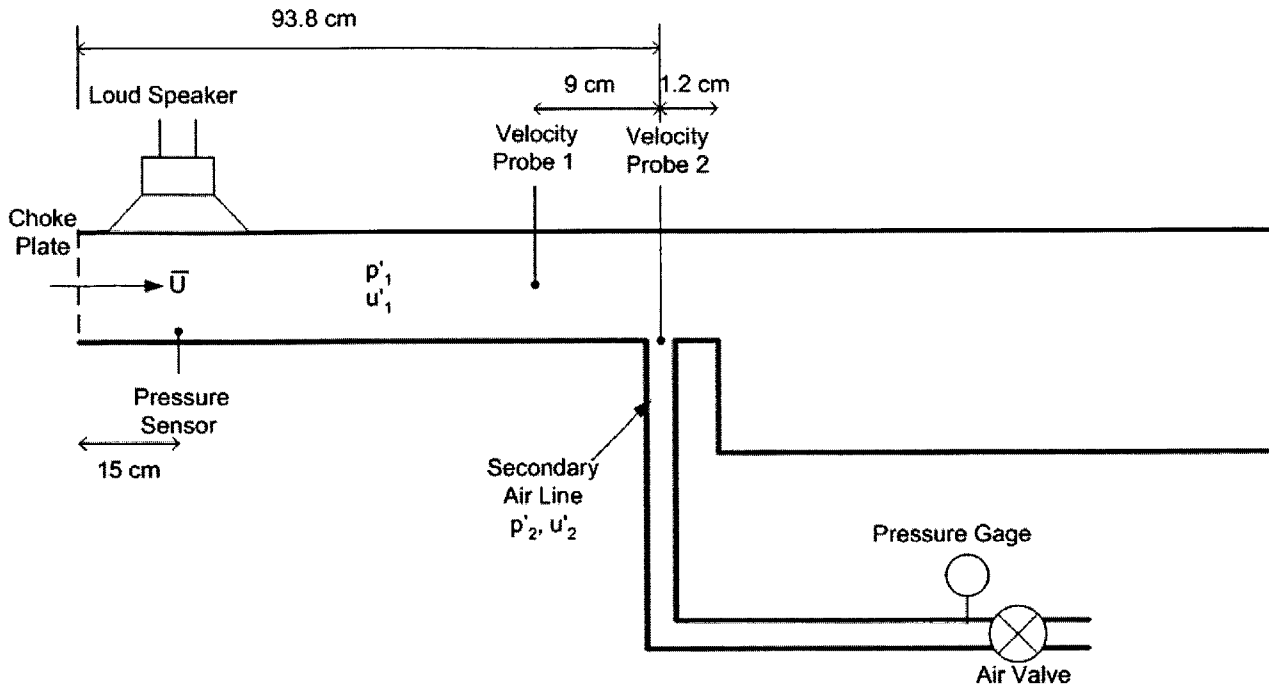


Figure 3-1: Schematic of experimental setup

the stability of the combustor.

### 3.1 Experimental Setup

The experimental test-bed is a backward facing step combustor providing a sudden expansion to stabilize the combustion, as shown in Fig. (3-1). It consists of a rectangular stainless steel duct with a cross section 40 mm high and 160 mm wide. The step height is 20 mm. The overall length of the combustor is 1.9 m, with the step located in the middle. The air inlet to the combustor is choked. The combustor is equipped with quartz viewing windows. An air compressor supplies air up to 110 g/s at 883 kPa. The sensors and actuators are positioned as indicated in the figure. In the figure,  $\bar{U}$  is the mean air velocity at the upstream,  $p'$  is the pressure oscillation,  $u'$  is the velocity oscillation and subscripts 1 and 2 refer to the primary channel and the secondary air line, respectively. The primary air velocity is measured 10.2 cm upstream of the step. The air injection velocity is measured just inside the air injection slot. Pressure fluctuation in the

primary channel is measured with the Kistler pressure sensors. The air mass flow meter is a Sierra Instruments 780S-NAA-N5-EN2-P2-V3-DD-0 Flat-Trak. The maximum flow rate is 173 g/s. The maximum pressure is 827 kPa. The unit is powered by an 18-30 V DC power supply, and it outputs a signal from 0-10 V DC, which is proportional to the mass flow rate of the air. Simultaneous velocity measurements are taken by TSI IFA-300 Hot Wire Anemometer. The actuation of the air from the slot is accomplished using Dynamco D1B2204 Dash 1 direct solenoid poppet air valves. This valve can supply 18 g/s of air when driven by 689 kPa. The valve is connected to a plenum beneath a 2 mm wide slot and 12 mm upstream of the step. An 80 W Radio Shack loud speaker is used to force the flow. It is connected to an Audio Source AMP 5.1A monoblock amplifier having a power output of 100W. The frequency response range is 20 Hz to 20 kHz.

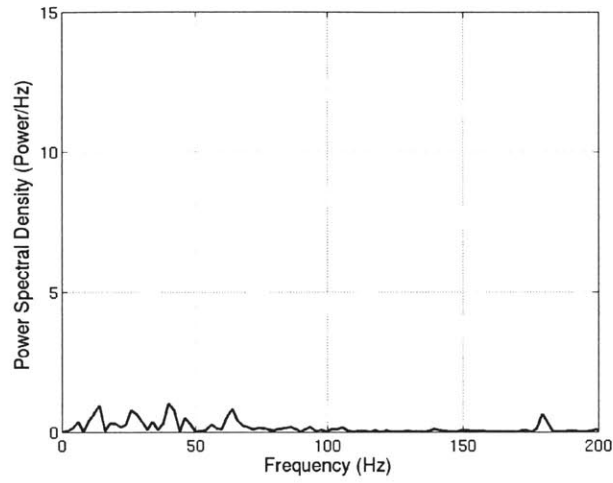
## 3.2 Experimental Results

Simultaneous velocity measurements are taken while varying the flow rate of the secondary jet and the amplitude of the acoustic forcing. The mean velocity of the primary stream,  $\bar{U}$ , the mean velocity of the jet,  $\bar{U}_j$ , and the forcing frequency,  $f$ , are kept at 3.7 m/s, 3.9 m/s and 40 Hz, respectively. Figure (3-2) compares the frequency spectrum of the secondary jet velocity at different forcing amplitudes. It is concluded that the pressure oscillations inside the combustor causes fluctuations in the secondary jet velocity. The amplitude of the pressure oscillations increases the oscillatory response of the secondary jet.

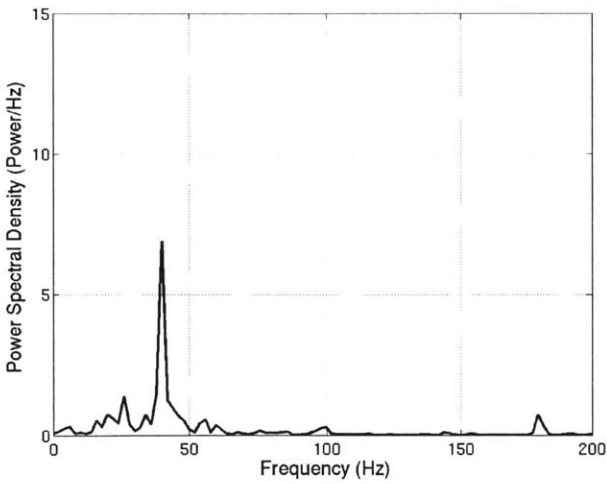
Next, I use measured velocities in order to illustrate the impact of the secondary jet on equivalence ratio. It is assumed that there is a fuel bar which is located just at the point where the primary stream velocity is measured, and the main fuel delivery line is choked such that the fuel flow is not oscillatory. The equivalence ratio at the fuel bar is given as:

$$\phi_{fb} = \frac{\dot{m}_f}{(u'_1(L_{fb}, t) + \bar{U})\bar{\rho}A_{cs}(F/A)_s} \quad (3.1)$$

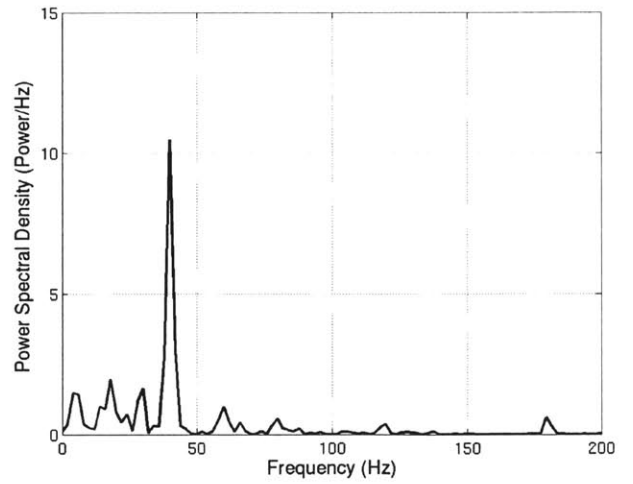
where  $\dot{m}_f$  is the mass flow rate of the fuel,  $\bar{\rho}$  is the mean air density,  $A_{cs}$  is the cross section area



(a) no forcing



(b) rms pressure amplitude=0.65kPa



(c) rms pressure amplitude=1.2 kPa

**Figure 3-2: Frequency spectra of jet velocity under different forcing amplitudes**

of the combustor,  $(F/A)_s$  is the stoichiometric fuel-air ratio of the fuel and  $L_{fb}$  is the distance between the fuel bar and the slot. The equivalence ratio oscillations formed in the fuel bar is simply convected to the secondary jet injection slot [56] and its oscillation amplitude decreases due to the effect of turbulent diffusion. The equivalence ratio at the slot without the presence of the secondary jet injection, with negligible turbulent diffusion is:

$$\phi_{s,nodif}^{w/o} = \frac{\dot{m}_f}{(u'_1(L_s, t - \tau_{convect}) + \bar{U})\bar{\rho}A_{cs}(F/A)_s} \quad (3.2)$$

where  $\tau_{convect}$  is the convection time scale, defined as  $\frac{L_{fb}}{\bar{U}}$ , and  $L_s$  is the location of the slot.

The effect of turbulent diffusion was shown to be very important in reducing the equivalence ratio oscillations [58]. Defining a correction factor for turbulent diffusion,  $\alpha$ , the equivalence ratio at the slot without the secondary air injection, including the effect of diffusion, is expressed as:

$$\phi_s^{w/o} = \phi_{s,nodif}^{w/o}\alpha - \bar{\phi}^{w/o}(\alpha - 1) \quad (3.3)$$

where  $\bar{\phi}^{w/o}$  is the mean equivalence ratio without the secondary air injection, i.e.,  $\bar{\phi}^{w/o} = \frac{\dot{m}_f}{\bar{\rho}A_{cs}\bar{U}(F/A)_s}$ . Note that,  $\alpha$  is in the range  $0 \leq \alpha \leq 1$ .  $\alpha = 0$  means that, diffusion is very strong so that all the oscillation is killed; on the other hand,  $\alpha = 1$  implies negligible diffusion. Substituting eqn. (3.2) into eqn. (3.3), the equivalence ratio at the slot without secondary jet is given as:

$$\phi_s^{w/o} = \frac{\dot{m}_f\alpha}{(u'_1(L_s, t - \tau_{convect}) + \bar{U})\bar{\rho}A_{cs}(F/A)_s} - \frac{\dot{m}_f(\alpha - 1)}{\bar{U}\bar{\rho}A_{cs}(F/A)_s} \quad (3.4)$$

With further simplification, eqn. (3.4) becomes:

$$\phi_s^{w/o} = \frac{\dot{m}_f}{\bar{U}\bar{\rho}A_{cs}(F/A)_s} \left[ \frac{\bar{U} + u'_1(L_s, t - \tau_{convect})(1 - \alpha)}{\bar{U} + u'_1(L_s, t - \tau_{convect})} \right] \quad (3.5)$$

With air injection, the new equivalence ratio is given as follows:

$$\phi_s^w = \frac{\dot{m}_f}{\bar{U}\bar{\rho}A_{cs}(F/A)_s \left[ \frac{\bar{U} + u'_1(L_s, t - \tau_{convect})}{\bar{U} + u'_1(L_s, t - \tau_{convect})(1 - \alpha)} \right] + \bar{\rho}A_j(F/A)_s[\bar{U}_j + u'_2(0, t)]} \quad (3.6)$$

where  $A_j$  is the cross section area of the secondary jet injection slot and  $u'_2(0, t)$  is the velocity of

the secondary jet at the slot. Note that, there is a delay,  $\tau_{ac}$ , between the secondary jet velocity and the primary air velocity, solely dependent on the acoustics of the combustor. Equation (3.6) suggests that the fluctuation in equivalence ratio will be minimum if the phase between  $u'_1(L_s, t - \tau_{convect})$  and  $u'_2(0, t)$  is zero. This requires:

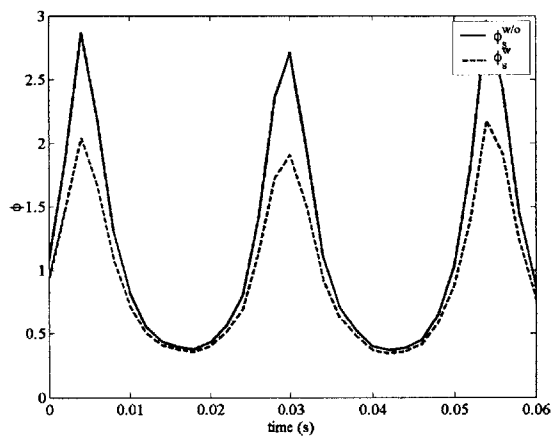
$$\tau_{convect} = \tau_{ac} + \frac{n}{f} \quad (3.7)$$

where  $n$  is an integer and  $f$  is the oscillation frequency in Hz.

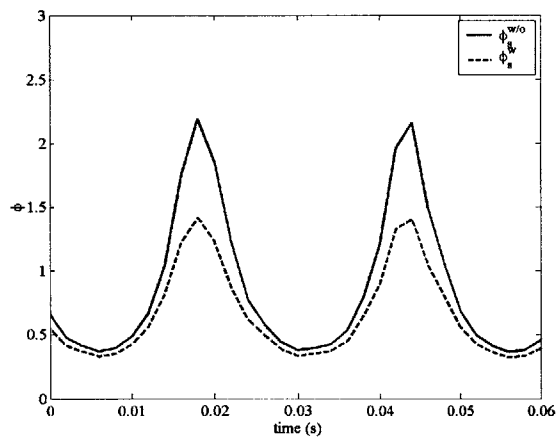
In Fig. (3-3), the effect of the secondary jet on the incoming equivalence ratio is examined using the measured velocities under constant amplitude forcing, i.e. rms of the forcing amplitude=0.65kPa. The values of the parameters in eqns. (3.2) and (3.6) are taken as:  $\dot{m}_f=0.66$  g/s,  $\bar{\rho}=1.29$  kg/m<sup>3</sup>,  $A_{cs}=32$  cm<sup>2</sup>,  $A_j=0.32$  cm<sup>2</sup>,  $L_{fb}=9$  cm,  $\alpha=0.5$  and  $(F/A)_s=0.0643$ , the value for propane. It is observed that, there is a significant reduction in equivalence ratio oscillation when I turn on the secondary jet. Also, the jet has no effect on the phase of the equivalence ratio oscillations. In order to have a better understanding of the effect of increasing jet velocity and turbulent diffusion on the reduction in oscillations, the percent reduction in normalized oscillation amplitude, i.e.  $\nu = \frac{\phi'_{rms}}{\phi}$ , as a function of the momentum ratio of the jet to the primary air, i.e.  $\beta = \frac{\rho \bar{U}^2}{\rho \bar{U}^2}$ , is plotted for various  $\alpha$  values in Fig. (3-4). It is observed that, as turbulent diffusion becomes more significant, i.e. as  $\alpha$  drops, the secondary jet has slightly less effect on reducing the normalized equivalence ratio oscillations. Also, increasing the jet velocity, increases the reduction in oscillations, as observed in (3-3).

These results demonstrate that the secondary jet has significant impact on the equivalence ratio. It should be noted that this non-reacting flow experiment is just a tool to demonstrate the validity of the proposed impact of the secondary jet in the combustor. The acoustics of a real combustor is different than what we have in this experiment. In a reacting flow, heat release rate oscillations act as a source of energy for the acoustics of the combustor that can generate self-sustained pressure oscillations. On the other hand, in this non-reacting experiment, the pressure oscillation is only a boundary condition which is generated by the loud speaker. Therefore, to investigate a reacting flow, an analytical model is required for the acoustics of the combustor

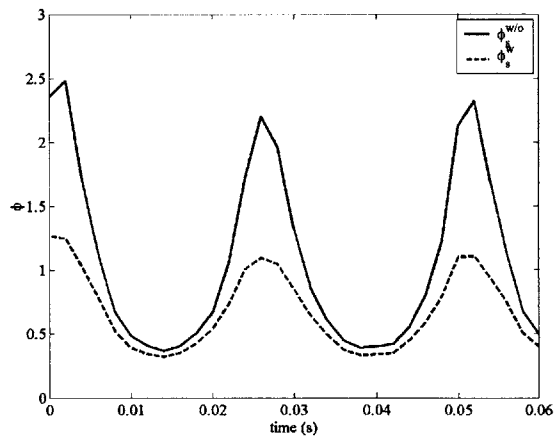




(a)  $\bar{U}_j=3.9$  m/s



(b)  $\bar{U}_j=7.7$  m/s



(c)  $\bar{U}_j=10.9$  m/s

Figure 3-3: Effect of air injection on equivalence ratio oscillations,  $\alpha=0.5$

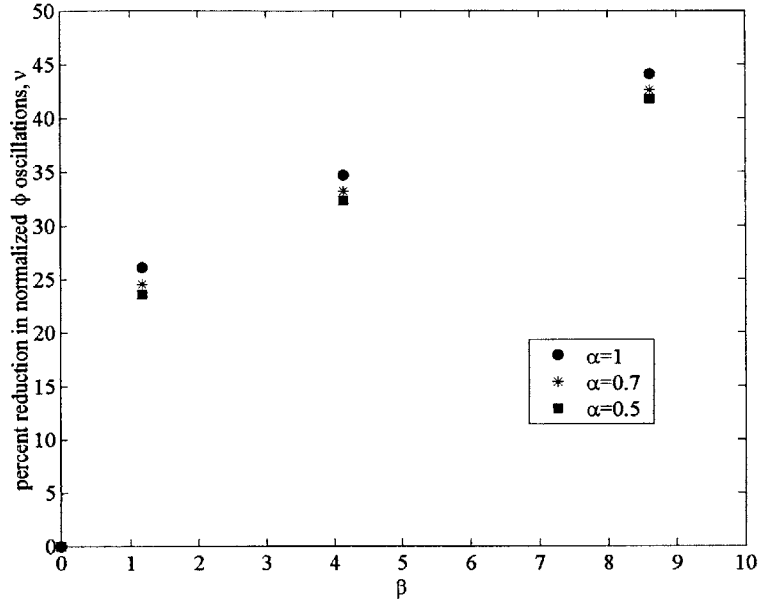


Figure 3-4: Percent reduction in normalized equivalence ratio oscillation amplitude,  $\nu$ , as a function of momentum ratio,  $\beta$

and the secondary air line, which is derived in the next section.

### 3.3 Modeling of Combustor Acoustics

#### 3.3.1 Modeling of the Combustor Channel

With heat addition per unit volume, the pressure perturbations in the combustor satisfy an inhomogeneous one-dimensional wave equation, assuming negligible mean flow ( $M \ll 1$ ), is given by:

$$\frac{1}{\bar{c}^2} \frac{\partial^2 p'_1}{\partial t^2} - \frac{\partial^2 p'_1}{\partial x^2} = \frac{\gamma - 1}{\bar{c}^2} \frac{\partial q'}{\partial t} \quad (3.8)$$

where  $\gamma$  is the specific heat ratio and  $\bar{c}$  is the mean speed of sound. Considering the unsteady heat input to be concentrated at a single axial plane  $x=b$ , the heat release rate per unit volume is expressed as [10]:

$$q'(x, t) = Q'(t)\delta(x - b) \quad (3.9)$$

where  $Q'(t)$  is the rate of heat input per unit area. Using this assumption, equation (3.8) reduces to the homogeneous wave equation in the regions  $x < b$  and  $x > b$ . Integration across  $x=b$  gives

$$p_1'(b^+, t) = p_1'(b^-, t) \quad (3.10)$$

and

$$u_1'(b^+, t) - u_1'(b^-, t) = \frac{\gamma - 1}{\rho \bar{c}^2} Q'(t) \quad (3.11)$$

Using an appropriate model for  $Q'(t)$ , eqn. (3.11) can be used to find the growth rate of the oscillations. This is outside of the scope of this study. I will use the amplitude of oscillations from the limit cycle amplitude measured in the experiments performed in the modeled combustor. The contribution of  $q'$  in the wave equation is canceled by an additional damping mechanism in the limit cycle behavior.

The solution of homogeneous wave equation can be written in the form:

$$p_1'(x, t) = f(t - x/\bar{c}) + g(t + x/\bar{c}) \quad (3.12)$$

where the functions  $f(t)$  and  $g(t)$  are arbitrary. From the one-dimensional form of linearized momentum equation:

$$u_1'(x, t) = (1/\rho \bar{c})[f(t - x/\bar{c}) - g(t + x/\bar{c})] \quad (3.13)$$

for perturbations of frequency  $\omega$ , it is convenient to write  $f(t) = \text{Re}[\hat{f} \exp(i\omega t)]$ , where the circumflex denotes a complex amplitude. With this notation:

$$\hat{p}_1(x) = \hat{f} \exp(-ikx) + \hat{g} \exp(ikx) \quad (3.14)$$

$$\hat{u}_1(x) = (1/\rho \bar{c})[\hat{f} \exp(-ikx) - \hat{g} \exp(ikx)] \quad (3.15)$$

where  $k$  is the wave number,  $k = \omega/\bar{c}$ .

In  $x < b$ , the solution of homogeneous wave equation that satisfies the inlet boundary condition  $\hat{u}_1(x) = 0$  is

$$\hat{p}_1(x) = A \cos(kx) \quad (3.16)$$

and

$$\hat{u}_1(x) = (-i/\bar{\rho}\bar{c})A\sin(kx) \quad (3.17)$$

where A is a complex constant. Similarly, in  $x > b$ , the boundary condition  $\hat{p}_1(L) = 0$ , where L is the total length of the combustor, leads to

$$\hat{p}_1(x) = B\sin[k(L - x)] \quad (3.18)$$

and

$$\hat{u}_1(x) = (i/\bar{\rho}\bar{c})B\cos[k(L - x)] \quad (3.19)$$

where B is also a complex constant. The pressure jump condition in equation (3.10) gives:

$$A\cos(kb) = B\sin[k(L - b)] \quad (3.20)$$

Substituting B from eqn. (3.20) into eqn. (3.18) and setting  $A\cos(kb)=C$ , the modeshapes are obtained as follows:

$$\hat{p}_1(x) = C \frac{\cos(kx)}{\cos(kb)} \quad (3.21)$$

for  $0 \leq x \leq b$ , and

$$\hat{p}_1(x) = C \frac{\sin[k(L - x)]}{\sin[k(L - b)]} \quad (3.22)$$

for  $x \leq b \leq L$ . C is an arbitrary constant. I am interested in the equivalence ratio fluctuations at the secondary air injection slot, that is in the  $x < b$  solution. The pressure and velocity oscillations in  $x < b$  are, respectively, given as:

$$p'_1(x, t) = C \frac{\cos(kx)}{\cos(kb)} \cos(\omega t) \quad (3.23)$$

$$u'_1(x, t) = \frac{C}{\bar{\rho}\bar{c}} \frac{\sin(kx)}{\cos(kb)} \sin(\omega t) \quad (3.24)$$

From experimental results, the pressure amplitude at  $x=15$  cm, i.e. the location of the pressure sensor, is known for a set of operating conditions. This information is used to determine the value of the constant C.

### 3.3.2 Modeling of the Secondary Air Line

The pressure gage, which is adjusted to set the air injection velocity at the step, measures highly oscillatory pressure, when the combustor operates under unstable conditions. This suggests that the acoustics of the secondary air line plays an important role in the combustion operation.

In the secondary air line I again need to solve the homogeneous wave equation. The pressure and velocity oscillations are  $p'_2(x, t)$  and  $u'_2(x, t)$ , respectively.  $x = 0$ , is the location of the injection slot. The boundary conditions are:

$$p'_2(0, t) = C \frac{\cos(L_s x)}{\cos(kb)} \cos(\omega t) \quad (3.25)$$

$$u'_2(L_j, t) = 0 \quad (3.26)$$

where  $L_j$  is the length of the secondary air line. The second boundary condition is a good approximation, since at the end of the secondary air line there is a valve restricting the passage of velocity oscillations. Using a similar methodology as before, the oscillating velocity component at the step is calculated as:

$$u'_2(0, t) = \frac{-C \tan(kL_j) \cos(kL_s)}{\bar{\rho} \bar{c} \cos(kb)} \sin(\omega t) \quad (3.27)$$

The velocity of injected air is:

$$u_2(0, t) = u'_2(0, t) + \bar{U}_j = \bar{U}_j - \frac{C \tan(kL_j) \cos(kL_s)}{\bar{\rho} \bar{c} \cos(kb)} \sin(\omega t) \quad (3.28)$$

When  $\bar{U}_j$  is small,  $u_2(0, t)$  is likely to have negative values during some part of a cycle. This means that the slot acts as a suction hole for the incoming mixture from upstream. During this part, the equivalence ratio in the primary flow will not experience a change. This has important effects on the overall equivalence ratio oscillations. The critical mean injection velocity below which suction will be observed is:

$$(\bar{U}_j)_{crit} = \frac{C \tan(kL_j) \cos(kL_s)}{\bar{\rho} \bar{c} \cos(kb)} \quad (3.29)$$

The critical momentum ratio for suction, i.e.  $\beta_{crit} = \frac{(\bar{U}_j)_{crit}^2}{\bar{U}^2}$ , becomes:

$$\beta_{crit} = \left[ \frac{C \tan(kL_j) \cos(kL_s)}{\bar{\rho} \bar{c} \cos(kb) \bar{U}} \right]^2 \quad (3.30)$$

### 3.3.3 Equivalence Ratio

Substituting eqns. (3.24) and (3.27) into eqns. (3.5) and (3.6), the equivalence ratio at the air injection slot, without and with the air injection are:

$$\phi_s^{w/o} = \frac{\dot{m}_f}{\bar{U} \bar{\rho} A_{cs} (F/A)_s} \left[ \frac{\bar{U} + \frac{C}{\bar{\rho} \bar{c}} \frac{\sin(kL_s)}{\cos(kb)} \sin(\omega t) (1 - \alpha)}{\bar{U} + \frac{C}{\bar{\rho} \bar{c}} \frac{\sin(kL_s)}{\cos(kb)} \sin(\omega t)} \right] \quad (3.31)$$

$$\phi_s^w = \frac{\dot{m}_f}{\bar{U} \bar{\rho} A_{cs} (F/A)_s \left[ \frac{\bar{U} + \frac{C}{\bar{\rho} \bar{c}} \frac{\sin(kL_s)}{\cos(kb)} \sin(\omega t)}{\bar{U} + \frac{C}{\bar{\rho} \bar{c}} \frac{\sin(kL_s)}{\cos(kb)} \sin(\omega t) (1 - \alpha)} \right] + \bar{\rho} A_j (F/A)_s \left[ \bar{U}_j - \frac{C}{\bar{\rho} \bar{c}} \frac{\tan(kL_j) \cos(kL_s)}{\cos(kb)} \sin(\omega t) \right]} \quad (3.32)$$

Equation (3.31) is used to calculate the equivalence ratio when  $\beta=0$ , and eqn. (3.32) is used for the range  $\beta \geq \beta_{crit}$ . In order to calculate the oscillatory component of equivalence ratio, the mean equivalence ratio, i.e.  $\bar{\phi} = \frac{\dot{m}_f}{[\bar{U} A_{cs} + \bar{U}_j A_j] \bar{\rho} (F/A)_s}$ , is subtracted from eqns. (3.31) and (3.32). Note that, without secondary air injection, the mean equivalence ratio becomes,  $\bar{\phi}^{w/o} = \frac{\dot{m}_f}{\bar{\rho} \bar{U} A_{cs} (F/A)_s}$ .

## 3.4 Modeling Results

To show the impact of the secondary jet, the rms of the amplitude of the equivalence ratio oscillations normalized by the mean equivalence ratio at the slot, with and without the secondary jet are calculated while increasing the mean velocity of the secondary jet and for various  $\alpha$ . Similar values as in Ref. [73] are used for the parameters in eqns. (3.31) and (3.32). These values are:  $\dot{m}_f=0.66$  g/s,  $C=1.8$  kPa,  $\bar{\rho}=1.29$  kg/m<sup>3</sup>,  $\bar{c}=410$  m/s,  $b=1.05$  m,  $\omega=251$  rad/s,  $L_{fb}=16.3$  cm,

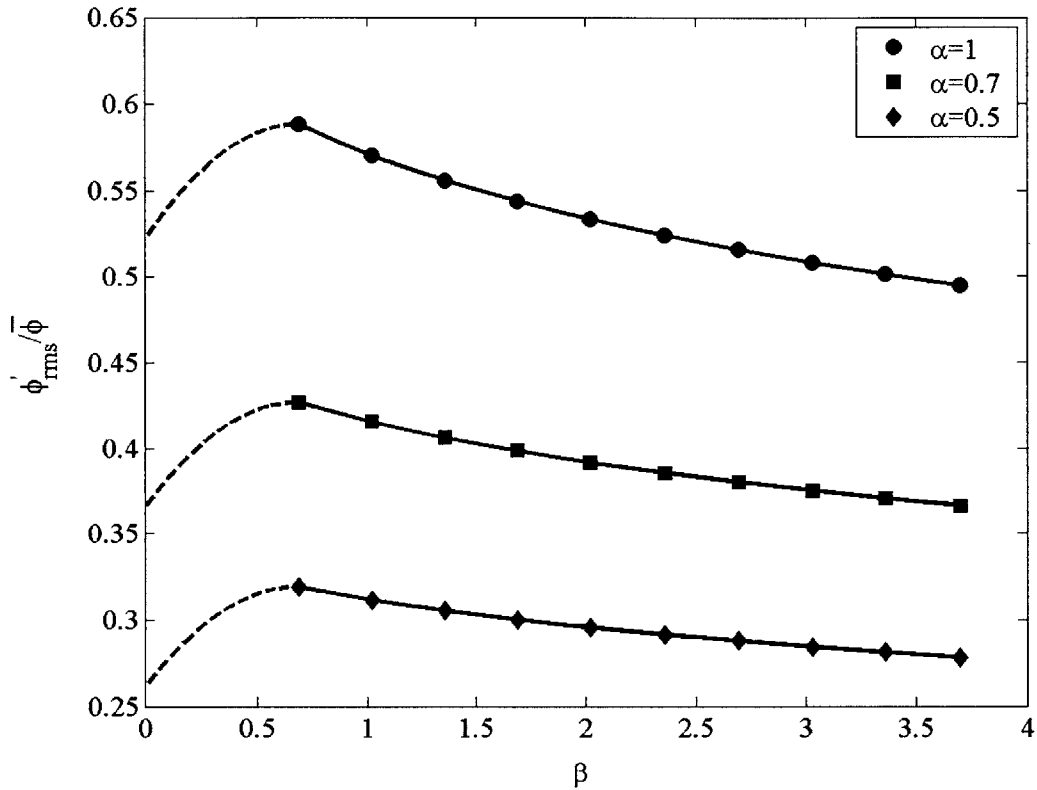


Figure 3-5: Normalized equivalence ratio oscillation amplitude,  $\nu$ , as a function of momentum ratio,  $\beta$ , for various  $\alpha$  values.

$L_j=1.3$  m,  $L_s=93.8$  cm,  $\bar{U}=4.4$  m/s,  $A_{cs}=32$  cm<sup>2</sup>,  $A_j=0.32$  cm<sup>2</sup> and  $(F/A)_s=0.0643$ .

First, the ratio,  $\frac{\tau_{convect}}{T}$  is calculated to determine whether the operating conditions correspond to an unstable band with respect to the equivalence ratio oscillations (see section 1.2.3).  $T$  is the oscillation period and  $\tau_{convect}$  is the convection time scale for equivalence ratio oscillations defined as  $\frac{L_{convect}}{\bar{U}}$  where  $L_{convect}$  is the distance between the fuel bar and the flame base, i.e. the step, which is 175 mm. This ratio is 1.59, which is in the unstable band, as shown in Fig. (1-14), for the case of a velocity node boundary condition. Therefore, equivalence ratio oscillations is proved to be a relevant mechanism for the formation of combustion instability for the above defined operating conditions.

Figure (3-5) shows the normalized equivalence ratio oscillation amplitude,  $\nu = \frac{\phi'_{rms}}{\phi}$ , at the slot, as a function of the momentum ratio of the secondary jet to the primary air,  $\beta$ , for various

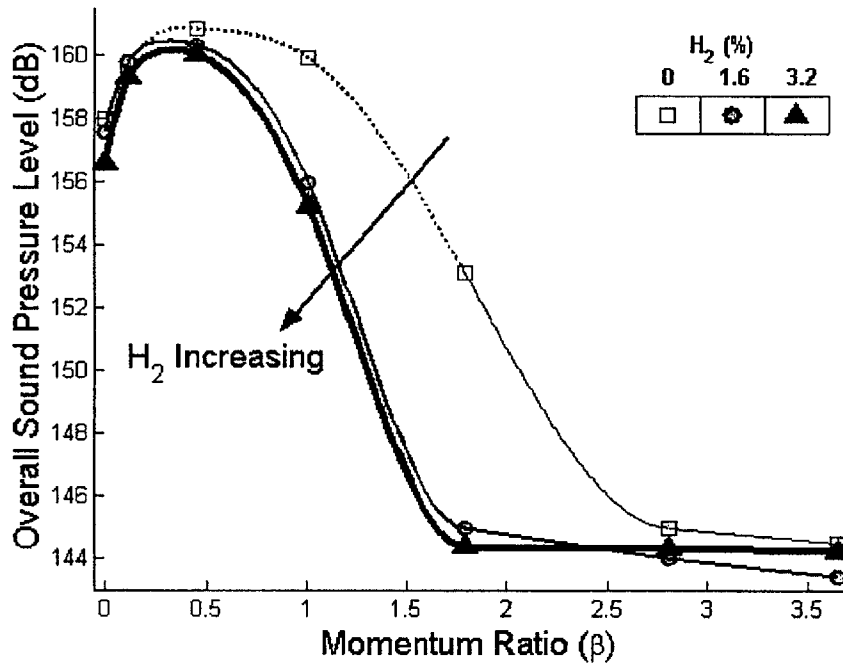
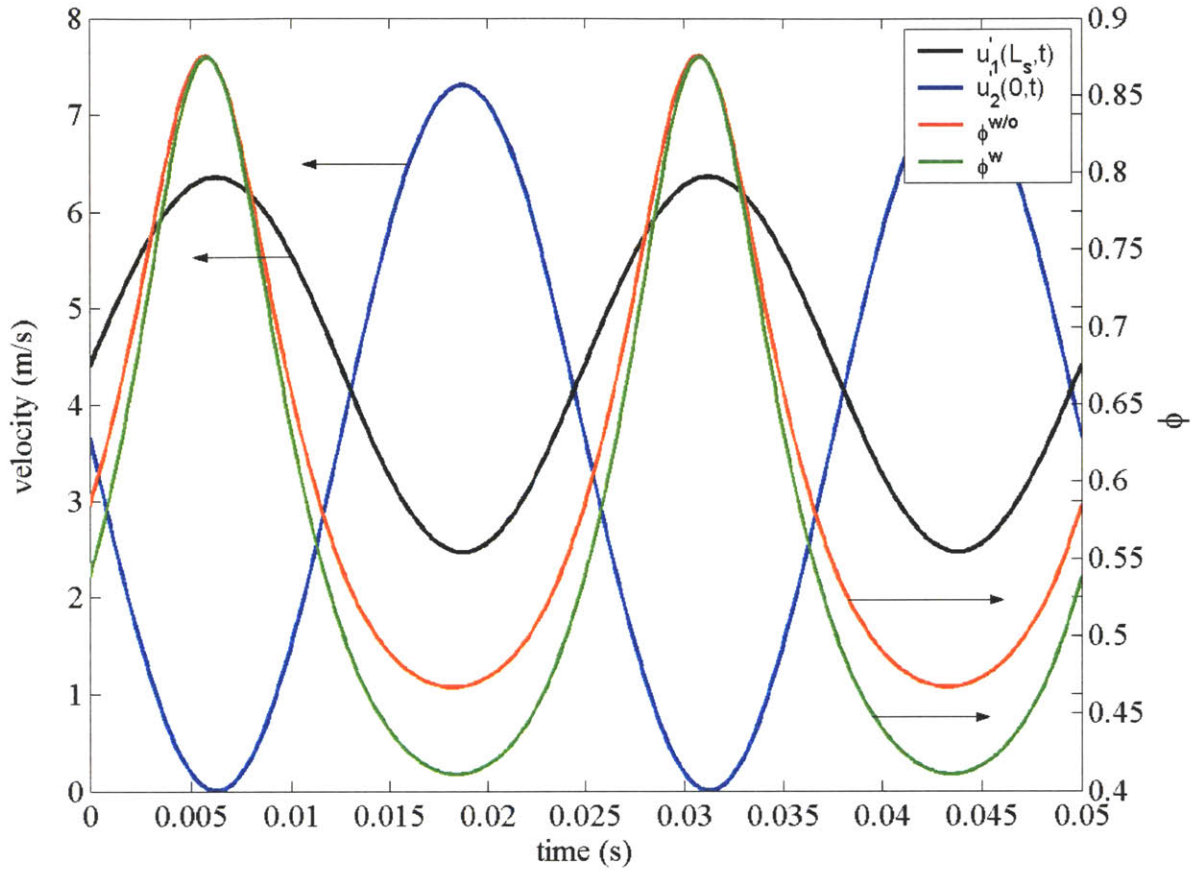


Figure 3-6: Dependence of the overall sound pressure level on the momentum ratio of the air injected near the step, for primary air velocity of 4.4 m/s, and fixed fuel flow rate of 0.66g/s. From Ref. [73]

values of  $\alpha$ . The sections shown in dashed lines correspond to  $\beta$  values less than the critical value defined in eqn. (3.30). Solution in that part requires numerical integration.

For  $\beta < \beta_{crit} = 0.69$ , there is suction of the incoming flow during part of the oscillation period. Even when the jet velocity is positive but small, jet-in-cross flow studies show that, because of the small velocity ratio of the secondary jet to the primary flow, the jet hardly penetrates into the stream, having a negligible impact on the fluid dynamics of the combustor. Therefore, in this range of momentum ratio, the only effect of the jet is on the equivalence ratio. During some part of the cycle, while the secondary jet velocity is negative, the mixture from the primary line is sucked into the slot. As the secondary jet velocity becomes positive, first the ingested mixture is injected back. Till the end of this time in the cycle, the overall equivalence ratio is not affected. From that moment until the end of the cycle, only air is injected from the slot, which increases the normalized equivalence ratio oscillation amplitude. As the momentum ratio increases, the duration for the air injection from the slot increases, which expands the





**Figure 3-7: Primary and secondary air velocities and equivalence ratio without and with the air injection at the location of the slot as a function of time when  $\beta = \beta_{crit}$  and  $\alpha = 0.5$ .**

time interval in the cycle during which the normalized equivalence ratio oscillation amplitude is negatively effected. Therefore, as the momentum ratio is increased from 0 to  $\beta_{crit}$ , the time interval for the air injection from the slot increases from 0 to the entire period, which increases  $\nu$ . The maximum oscillation amplitude is observed at  $\beta_{crit}$ , beyond which no suction of the primary jet is observed. This result matches with the experimental findings in Ref. [73] in the modeled combustor, presented in Fig. (3-6), which shows that the overall sound pressure level reaches a maximum when momentum ratio is around 0.5, independent of the mixture composition. It is also observed that as the turbulent diffusion effect increases, i.e. as  $\alpha$  decreases, the negative impact of the suction on equivalence ratio oscillation amplitude decreases. Figure (3-7) shows the primary and secondary air velocities and equivalence ratio without and with the air injection

at the location of the slot as a function of time, when  $\beta = \beta_{crit}$  and  $\alpha = 0.5$ . It is observed that the equivalence ratio is negatively effected from the jet, as expected. Near the lean flammability limit, the equivalence ratio with the secondary jet shows around 15 percent higher oscillation compared to the equivalence ratio when there is no air injection. This leads to an increase in the instability of the combustor compared to the operation without the secondary jet.

There is another mechanism which contributes to the increase in the instability observed when  $\beta < \beta_{crit}$ . During the suction interval, some of the mass from the primary channel enters the secondary air line, so the mass flow rate reaching the combustion zone is less than the mass flow rate at the upstream of the primary channel. As the velocity becomes positive, the mass flow rate of the mixture entering the combustion zone becomes higher than the mass flow rate at the upstream. Therefore, in this momentum ratio range, the average mass flow rate entering the combustion zone oscillates, resulting in unsteady heat release rate, which causes instability.

In summary, these results demonstrate that when the momentum ratio is around the critical value defined as the minimum momentum ratio to prevent suction of the fluid in the primary channel, the secondary jet injection has the most negative effect on the combustor stability because the normalized equivalence ratio oscillation amplitude reaches its maximum. As the momentum ratio is increased beyond the critical value, the equivalence ratio oscillation amplitude decreases. However, Fig. (3-5) shows that, even when the momentum ratio reaches high values, the normalized equivalence ratio oscillation amplitude is still comparable to the case without secondary air injection. Therefore, the sudden drop in the overall sound pressure level observed in Fig. (3-6) for momentum ratio around 2-2.5 cannot be explained by the effect of the secondary jet on equivalence ratio. This suggests that, for this combustor, the equivalence ratio acts as a secondary mechanism for combustion instability. Park [58] reached the same conclusion after performing experiments in the same combustor. He observed unstable combustion with significant flame-vortex interaction, even when there were no equivalence ratio oscillations at the flame (see section 1.2.3). Therefore, the sudden drop in the overall sound pressure level observed in Fig. (3-6) can be explained by the positive impact of the secondary jet on the flame-vortex interaction mechanism. One possible effect of the jet is deflecting the primary stream away from the lower wall, preventing the formation of the wake vortex at the step at high enough momentum

ratios. This effect will be investigated in detail in later studies.

### 3.5 Summary

In this chapter, I investigated the effect of air injection in cross stream direction on equivalence ratio oscillations. It was shown that high amplitude pressure oscillations in the combustor during unstable operation caused the secondary jet velocity to oscillate. This oscillation effects the incoming equivalence ratio oscillations depending on the relative amplitude and phase between the oscillations and the momentum ratio of the secondary jet to the primary stream. I found that when the momentum ratio was less than a critical value, the air injection slot acted as a suction to the incoming stream. When the momentum ratio was greater than that critical value, the normalized amplitude of equivalence ratio oscillations decreased with increasing momentum ratio. The maximum normalized equivalence ratio oscillation amplitude was observed at the critical momentum ratio, the value of which matched with the previous experimental observations. It was concluded that, the sudden drop of the overall sound pressure level observed in previous experiments could not be explained by the effect of the secondary jet on equivalence ratio. This suggests that equivalence ratio oscillations is a secondary instability mechanism for the combustor, the primary mechanism being the flame-vortex interactions. The sudden drop can be explained with a possible effect of the secondary jet on preventing the formation of the unsteady vortex at the step. This effect will be explained further in later studies.

# Chapter 4

## Conclusions

In this thesis, first, I reviewed combustion dynamics in detail by explaining the elementary mechanisms causing unsteady heat release during the combustion process. Among those mechanisms, the flame vortex-interactions and equivalence ratio oscillations are most relevant to lean premixed combustion. In simple terms, the former causes oscillations in the flame surface area and the latter results in variations of the local burning rate, both of which contributing to heat release rate oscillations.

Next, I investigated the flame-vortex interactions numerically in single and double expansion dump combustors and related the heat release rate response to the incoming velocity oscillations by performing a parametric study. I found that the combustor geometry, Strouhal number and the non-dimensional laminar burning velocity,  $S_u$ , are key parameters determining whether the combustor will operate in the unstable mode. The geometry of the combustor determines the moment in the cycle when the vortex breakup is initiated. A short time after the vortex breakup, the maximum heat release rate is reached. Therefore, the geometry plays an important role in determining the phase between the heat release rate and pressure oscillations, i.e., the operating mode of the combustor. For short cavities, vortex breakup is initiated as the large wake vortex collides with the forward-facing step of the combustor. On the other hand, in long cavities the vortex never reaches the forward-facing step. The vortex breakup is initiated as the vortex collides with the other vortex structure formed in the other half of the combustor in

double expansion dump combustors, or the upper wall of the channel in single expansion dump combustors. I observed that the time when the maximum heat release rate was reached was longer in long cavity combustors. This makes long cavity combustors more prone to combustion instability because of the Rayleigh's criterion. Also, as the Strouhal number is decreased, the combustor operation shifts through the stable operating band. Increasing the non-dimensional laminar burning velocity, i.e. equivalence ratio, the critical Strouhal number above which the combustor will be unstable increases.

Finally, I studied the effect of secondary air injection in cross stream direction on equivalence ratio in a backward-facing step combustor. First non-reacting experiments were performed to validate the effect of air injection on equivalence ratio oscillations. I observed that the pressure oscillations generated in the combustor caused oscillations in the injected air velocity. As this oscillatory jet interacts with the equivalence ratio in the primary channel, the magnitude of the resulting equivalence ratio oscillation may increase or decrease depending on the phase between the secondary jet velocity and the initial equivalence ratio, their relative oscillation amplitude and the momentum ratio of the secondary jet to the primary flow. After validating the mechanism, I modeled the acoustics of the combustor and the secondary air line to gain further insight into the mechanism. For a set of operating conditions, which were also used in the previous experimental studies, I found that as the momentum ratio of the secondary jet to the primary flow was at a critical value, the equivalence ratio oscillation amplitude normalized with respect to its mean value reached a maximum. This explains the peak in the overall sound pressure level measured in previous experiments around a critical momentum ratio. The critical momentum ratio is the momentum ratio below which suction of the incoming velocity into the slot is observed during part of the oscillation period. As the momentum ratio was increased above the critical value, the normalized equivalence ratio amplitude decreased. However, the normalized equivalence ratio amplitude was still comparable to the value when there was no secondary air injection. This suggests that the drop in the overall sound pressure level observed in the experiments around momentum ratio 2-2.5 cannot be explained by the effect of the secondary jet on equivalence ratio alone. Most likely, the jet at that range of momentum ratio, lifts the primary flow upwards preventing the formation of the large wake vortex. This prevents the flame-vortex interactions,

which was shown to be the primary instability mechanism in the modeled combustor. Future work will focus on the investigation of the effect of the secondary jet on flame-vortex interaction mechanism.

# Bibliography

- [1] S. Candel. Combustion dynamics and control: Progress and challenges. *Proceedings of the Combustion Institute*, 29:1, 2002.
- [2] J.W.S. Rayleigh. *The Theory of Sound*, 2:232, 1896.
- [3] G.A. Richards, G.J. Morris, D.W. Shaw, S.A. Keely, and M.J. Welter. Thermal pulse combustion. *Combustion Science and Technology*, 94:93, 1993.
- [4] M.C. Janus and G. Richards. Results of a model for premixed combustion oscillations. *Proceedings of the 1996 Meeting of the American Flame Research Council*, 1996.
- [5] S. Park, A. Annaswamy, and A. Ghoniem. Heat release dynamics modeling of kinetically controlled burning. *Combustion and Flame*, 128(5):217, 2002.
- [6] T. Lieuwen, Y. Neumeier, and B.T. Zinn. The role of unmixedness and chemical kinetics in driving combustion instabilities in lean premixed combustors. *Combustion Science and Technology*, 135:193, 1998.
- [7] A.F. Ghoniem, A. Annaswamy, D. Wee, T. Yi, and S. Park. Shear-flow driven combustion instability: Evidence, simulation, and modeling. *Proceedings of the Combustion Institute*, 29:53, 2002.
- [8] D. Wee, S. Park, T. Yi, A. Annaswamy, and A. Ghoniem. Reduced order modeling of reacting shear flow. *40th AIAA Aerospace Sciences Meeting Conference and Exhibit*, 2002.

- [9] D. Wee, T. Yi, A. Annaswamy, and A.F. Ghoniem. self-sustained oscillations and vortex shedding in backward-facing step flows: Simulation and linear stability analysis. *Physics of Fluids*, 16(9):3361, 2004.
- [10] A.P. Dowling and S.R. Stow. Acoustic analysis of gas turbine combustors. *Journal of Propulsion and Power*, 19(5):751, 2003.
- [11] K.I. Matveev and F.E.C. Culick. A model for combustion instability involving vortex shedding. *Combustion Science and Technology*, 175:1059, 2003.
- [12] C. Pankiewicz and T. Sattelmayer. Time domain simulation of combustion instabilities in annular combustors. *Journal of Engineering for Gas Turbines and Power*, 125:677, 2003.
- [13] T. Lieuwen. Modeling premixed combustion - acoustic wave interactions: A review. *Journal of Propulsion and Power*, 19(5):765, 2003.
- [14] B.T. Chu. On the generation of pressure waves at a plane flame front. *Fourth Symp. (Intl) on Combustion*, page 603, 1953.
- [15] T. Lieuwen. Theoretical investigation of unsteady flow interactions with a premixed planar flame. *Journal of Fluid Mechanics*, 435:289, 2001.
- [16] T. Lieuwen. Theory of high frequency acoustic wave scattering by turbulent flames. *Combustion and Flame*, 126:1489, 2001.
- [17] T. Lieuwen. Analysis of acoustic wave interactions with turbulent premixed flames. *Proceedings of the Combustion Institute*, 29:1817, 2002.
- [18] T. Lieuwen, Y. Neumeier, and R. Rajaram. Measurements of incoherent acoustic wave scattering from turbulent premixed flames. *Proceedings of the Combustion Institute*, 29:1809, 2002.
- [19] A. Laverdant and D. Thevenin. Interaction of a gaussian acoustic wave with a turbulent premixed flame. *Combustion and Flame*, 134:11, 2003.



- [20] A.C. McIntosh. Deflagration fronts and compressibility. *Philosophical Transactions of the Royal Society of London*, 357:3523, 1999.
- [21] A.C. McIntosh. Pressure disturbances of different length scales interacting with conventional flames. *Combustion science and Technology*, 75:287, 1991.
- [22] H.J. Merk. An analysis of unstable combustion of premixed gases. *Sixth Symp. (Intl) on Combustion*, page 500, 1956.
- [23] R. Becker and R. Gunther. The transfer function of premixed turbulent jet flames. *Thirteenth Symp. (Intl) on Combustion*, page 517, 1971.
- [24] Y. Matsui. An experimental study on pyro-acoustic amplification of premixed laminar flames. *Combustion and Flame*, 43(2):199, 1981.
- [25] G.H. Markstein. Theory of flame propagation. *Nonsteady flame Propagation*, 1964.
- [26] M. Fleifil, A.M. Annaswamy, Z.A. Ghoniem, and A.F. Ghoniem. Response of a laminar premixed flame to flow oscillations: A kinematic model and thermoacoustic instability results. *Combustion and Flame*, 106:487, 1996.
- [27] S. Ducruix, D. Durox, and S. Candel. Theoretical and experimental determinations of the transfer function of a laminar premixed flame. *Proceedings of the Combustion Institute*, 28:765, 2000.
- [28] T. Schuller, D. Durox, and S. Candel. A unified model for the prediction of laminar flame transfer functions: comparisons between conical and v-flame dynamics. *Combustion and Flame*, 134:21, 2003.
- [29] D.H. Lee and T.C. Lieuwen. Premixed flame kinematics in a longitudinal acoustic field. *Journal of Propulsion and Power*, 19(5):837, 2003.
- [30] D. H. Lee and T.C. Lieuwen. Acoustic nearfield characteristics of a conical, premixed flame. *Journal of the Acoustical Society of America*, 113(1), 2003.

- [31] T. Schuller, S. Ducruix, D. Durox, and S. Candel. Modeling tools for the prediction of premixed flame transfer functions. *Proceedings of the Combustion Institute*, 29:107, 2002.
- [32] B.T. Zinn and E.A. Powell. *Proc. Comb. Inst.*, 13, 1970.
- [33] F.E.C. Culick. *Combustion Science and Technology*, 3, 1971.
- [34] A. Bourehla and F. Baillot. Appearance and stability of a laminar conical flame subjected to an acoustic perturbation. *Combustion and Flame*, 114(3):303, 1998.
- [35] A.P. Dowling. A kinematic model of a ducted flame. *Journal of Fluid Mechanics*, 394:51, 1999.
- [36] T. Lieuwen and Y. Neumeier. Nonlinear pressure-heat release transfer function measurements in a premixed combustor. *Proceedings of the Combustion Institute*, 29:99, 2002.
- [37] B.D. Bellows, Q. Zhang, Y. Neumeier ad T. Lieuwen, and B.T. Zinn. Forced response studies of a premixed flame to flow disturbances in a gas turbine combustor. *41st AIAA Aerospace Sciences Meeting and Exhibit, Reno, NV*, 2003.
- [38] P.H. Renard, D. Thevenin, J.C. Rolon, and S. Candel. Dynamics of flame/vortex interactions. *Progress in energy and Combustion Science*, 26:225, 2000.
- [39] A.E. Noreen W.E. Kaskan. High-frequency oscillations of a flame held by a bluff body. *ASME Trans.*, 77:885, 1955.
- [40] D.E. Rogers and F.E. Marble. A mechanism for high-frequency oscillations in ramjet combustors and afterburners. *Progress in energy and Combustion Science*, 18:117, 1956.
- [41] T. Poinso, A. Trouve, D. Veynante, S. Candel, and E. Esposito. Vortex-driven acoustically coupled combustion instabilities. *Journal of Fluid Mechanics*, 177:265, 1987.
- [42] K. Schadow and E. Gutmark. Large-scale coherent structures as drivers of combustion instability. *Combustion Science and Technology*, 64:167, 1989.
- [43] J.D. Sterling and E.E. Zukowski. Nonlinear dynamics of laboratory combustor pressure oscillations. *Combustion Science and Technology*, 77:225, 1991.

- [44] K.H. Yu, A. Trouve, and J.W. Daily. Low-frequency pressure oscillations in a model ramjet combustor. *Journal of Fluid Mechanics*, 232:47, 1991.
- [45] K.K. Venkataraman, B.J. Lee L.H. Preston, D.W. Simons, J.G. Lee, and D.A. Santavicca. Mechanism of combustion instability. *Journal of Propulsion and Power*, 15(6):909, 1999.
- [46] A.F. Ghoniem, A.M. Annaswamy, S. Park, D. Wee, Z. Sobhani, and M. Altay. Model-based optimal active control of liquid fueled combustion systems. *Seventeenth ONR Propulsion Meeting, Cambridge, MA*, 2004.
- [47] D. Bernier, F. Lacas, and S. Candel. Instability mechanisms in a premixed prevaporized combustor. *Journal of Propulsion and Power*, 20(4):648, 2004.
- [48] D.W. Kendrick, T.W. Zsak, and E.E. Zukowski. An experimental and numerical investigation of premixed combustion in a vortex in a laboratory dump combustors. *Unsteady Combustion, North Atlantic Treaty Organization Advanced Science Institute Series*, 306:33, 1996.
- [49] Y. Huang, H.G. Sung, S.Y. Hsieh, and V. Yang. Large-eddy simulation of combustion dynamics of lean-premixed swirl-stabilized combustor. *Journal of Propulsion and Power*, 19(5):782, 2003.
- [50] H.N. Najm and A.F. Ghoniem. Coupling between vorticity and pressure oscillations in combustion instability. *Journal of Propulsion and Power*, 10(6):769, 1994.
- [51] D. Thibaut and S. Candel. Numerical study of unsteady turbulent premixed combustion: Application to flashback simulation. *Combustion and Flame*, 113:53, 1998.
- [52] C. Fureby. A computational study of combustion instabilities due to vortex shedding. *Proceedings of the Combustion Institute*, 28:783, 2000.
- [53] T. Lieuwen and B.T. Zinn. The role of equivalence ratio oscillations in driving combustion instabilities in low nox gas turbines. *Proceedings of the Twenty-seventh International Symposium on Combustion*, 27:1809, 1998.

- [54] J.G. Lee, K. Kwanwoo, and D.A. Santavicca. Measurement of equivalence ratio fluctuation and its effect on heat release during unstable combustion. *Proceedings of the Combustion Institute*, 28:1809, 1998.
- [55] A.A. Peracchio and W.M. Proscia. Nonlinear heat-release/ acoustic model for thermoacoustic instability in lean premixed combustors. *Journal of Engineering for Gas Turbines and Power*, 121:415, 2000.
- [56] T. Lieuwen, H. Torres, C. Johnson, and B.T. Zinn. A mechanism of combustion instability in lean premixed gas turbine combustors. *Journal of Engineering for Gas Turbines and Power*, 123:182, 2001.
- [57] G.M. Abu-Off and R.S. Cant. Reaction rate modeling for premixed turbulent methane-air flames. *Proc. Joint Meeting of Spanish, Portuguese, Swedish and British Sections of the Combustion Institute*, 1996.
- [58] S. Park. Active combustion control : Modeling, design and implementation. *PhD Dissertation, MIT*, June 2004.
- [59] T. Schuller, D. Durox, and S. Candel. Dynamics of and noise radiated by a perturbed impinging premixed jet flame. *Combustion and Flame*, 128:88, 2002.
- [60] D. Durox, T. Schuller, and S. Candel. Self-induced instability of a premixed jet flame impinging on a plate. *Proceedings of the Combustion Institute*, 29:69, 2002.
- [61] Y. Zhang and K.N.C. Bray. Characterization of impinging jet flames. *Combustion and Flame*, 116:671, 1999.
- [62] C.K. Law and C.J. Sung. Structure, aerodynamics, and geometry of premixed flamelets. *Progress in Energy and Combustion Science*, 26:459, 2000.
- [63] T. Poinso, T. Echekeki, and M.G. Mungal. A study of the laminar flame tip and implications for premixed turbulent combustion. *Combustion Science and Technology*, 81:45, 1991.
- [64] P. Clavin and G. Joulin. Premixed flames in large-scale and high-intensity turbulent-flow. *Journal de Physique Lettres*, 44, 1983.

- [65] C.K. Law. Dynamics of stretched flames. *Proceedings of the Twenty-Second International Symposium on Combustion*, page 1381, 1988.
- [66] T. Echekki and J.H. Chen. Unsteady strain rate and curvature effects in turbulent premixed methane-air flames. *Combustion and Flame*, 106:203, 1996.
- [67] J.H. Chen and H.G. Im. Stretch effects on the burning velocity of turbulent premixed hydrogen-air flames. *Proceedings of the Combustion Institute*, 28:211, 2000.
- [68] H.G. Im, J.K. Bechtold, and C.K. Law. Response of counterflow premixed flames to oscillating strain rates. *Combustion and Flame*, 105:358, 1996.
- [69] C.A. Petrov and A.F. Ghoniem. The transient response of strained laminar-premixed flames. *Combustion and Flame*, 102:401, 1995.
- [70] S. Ducruix, T. Schuller, D. Durox, and S. Candel. Combustion dynamics and instabilities: elementary coupling and driving mechanisms. *Journal of Propulsion and Power*, 19(5):722, 2003.
- [71] H.N. Najm. Numerical investigation of the instability of premixed dump combustors. *Ph.D. Dissertation, MIT*, 1989.
- [72] Ahmed F. Ghoniem, S. Park, A. Wachsman, A. Annaswamy, D. Wee, and H.M. Altay. Mechanism of combustion dynamics in a backward-facing step stabilized premixed flame. *Proceedings of the Combustion Institute*, 30:1783, 2004.
- [73] A.F. Ghoniem, A. Annaswamy, S. Park, and Z. Sobhani. Stability and emissions control using air injection and h<sub>2</sub> addition in premixed combustion. *Proceedings of the Combustion Institute*, 30:1765, 2005.